THESIS

EVALUATING THE FREQUENCY, SIZE, AND DURATION OF DUST STORMS IN THE UNITED STATES USING SATELLITE AND SURFACE DATA

Submitted by

Jennifer M. McGinnis

Department of Atmospheric Science

In partial fulfillment of the requirements

For the Degree of Master of Science

Colorado State University

Fort Collins, Colorado

Fall 2025

Master's Committee:

Advisor: Jeffrey R. Pierce
Co-Advisor: Emily V. Fischer

Steven D. Miller
Sheryl Magzamen

ABSTRACT

EVALUATING THE FREQUENCY, SIZE, AND DURATION OF DUST STORMS IN THE UNITED STATES USING SATELLITE AND SURFACE DATA

The United States (US) experiences frequent dust storms that are primarily identified using ground-based monitoring networks. However, current ground monitor networks are unable to capture the full extent of a dust event due to limited spatial coverage. Leveraging satellite data can help bridge these gaps in surface in situ data. Using the GOES-East geostationary satellite and a longwave-based satellite algorithm, we have identified dust events and evaluated the algorithm against surface-level air quality data. This work provides a novel evaluation of satellite-identified dust products for surface-level dust in the US. We found that these satellite data miss the vast majority of dust events observed by surface monitors, only correctly identifying 9.2% of elevated (>330 μg m^{-3}) coarse particulate matter (PM_{coarse}; particulate matter with diameters >2.5 μm and <10 μm) concentration events in the contiguous US. Conversely, over 90% of the satellite-observed dust storms occur further than 10 km from monitoring stations. Although there were more frequent dust events in the Southwest US, dust events over the South Central US tend to be larger and last longer, according to satellite data from 2018-2023. In the Southwest, 0.69% of satellite-identified dust events (14 events) reached a maximum area of 10,000 km^2 and in the South Central, 6.0% of dust events (53 events) reached 10,000 km^2. Additionally, 8.7% (177 events) of dust storms in the Southwest and 16% of (142 events) dust storms in the South Central lasted longer than 5 hours. This analysis implies that large dust events are prevalent in the US and the existing monitoring networks fail to capture a substantial portion of them, highlighting the need for additional data sources and more comprehensive networks.

ACKNOWLEDGEMENTS

I would like to thank my graduate advisors, Dr. Jeffrey R. Pierce and Dr. Emily V. Fischer for their continued support and guidance throughout this work. They have continued to push me to be the best scientist I can be and explore exciting research. I also want to thank my committee members, Dr. Sheryl Magzamen and Dr. Steven D. Miller, for their expertise and for serving on my committee.

I would also like to thank everyone I overlapped with in the Pierce and Fischer research groups: Olivia Sablan, Sam O'Donnell, Nicole June, En Li, Brandon McGuire, Ana Elizabeth Lasso de la Vega Guerra, Hannah Grace Marti, Dr. Haihui Zhu, Dr. Margot Clyne, Milena Guajardo, Madison Shogrin, Dr. Kimberley Corwin, Emily Lill, Lena Low, Daniela Guevara, Dr. Julietta Juncosa, and Dr. Matthew Davis. Their ongoing support has been essential for my success.

I would like to thank my undergraduate mentor, Dr. Tracey Holloway, for opening the door for me to pursue air quality research. My time in her research group was one of the most transformative chapters of my life and allowed me to fall in love with air quality research.

Without my family and friends none of this would be possible. I would like to thank my mom and dad, Rose and Mike, as well as my sister, Laura, for being my biggest cheerleaders, coming to visit me, and offering unwavering emotional support throughout this journey. My brother-in-law, Sam, and my niece, Jada, for supplying me with cute baby pictures as I write this thesis. My partner Dennis for supporting me, making me coffee, and listening to my research even when I start rambling about dust detection and infrared wavelengths and emissivity and brightness temperatures. Thank you to my friends from Wisconsin: Jordan, Julia, Kelly, Sam, and Megan for being my outlet to talk about anything and everything and for being the best support system. Thank

you to all of the people I have met in Fort Collins for making my move here an easy adjustment and for making my first two years here incredible.

Finally, thank you to the NASA Health and Air Quality Team for making this research possible through the NASA grant #80NSSC21K0429.

TABLE OF CONTENTS

CHAPTER 1: INTRODUCTION

In most regions of the contiguous United States (CONUS), dust is the main component of coarse particulate matter (PM_{coarse}, particulate matter with diameters > 2.5 μm and < 10 μm) (Hand et al., 2017, 2019; Kumar et al., 2012; Malm et al., 2007; D. Q. Tong et al., 2012). Major sources of dust PM_{coarse} include agricultural fields, arid land, deserts, unpaved roads, and construction sites (Hand et al., 2017, 2019; Malm & Hand, 2007; Masri et al., 2015; Sprigg et al., 2022; D. Q. Tong et al., 2017). PM_{coarse} causes respiratory morbidity, cardiovascular morbidity, non-accidental mortality, and infectious diseases, and it has been estimated that premature deaths due to dust exposure results in $13 billion per year (Achakulwisut et al., 2019; Chen et al., 2019; Crooks et al., 2016; Kodros et al., 2018; Liu, Cai, et al., 2022; D. Q. Tong et al., 2017). Additionally, the infectious disease, Valley Fever, has thousands of cases reported a year and has been correlated with the frequency of dust storms due to dust serving as a carrier for fungi (Prospero et al., 2005; Sprigg et al., 2022; D. Q. Tong et al., 2017). Although many studies have documented long-range transport of dust to the CONUS from the Asian and African continents (Fischer et al., 2009; Perry et al., 1997; Prospero, 1999b), the data available for dust storms and PM_{coarse} events in the CONUS is limited, which creates uncertainty in the extent of the full scope of dust-related health impacts. The lack of data also hinders public warnings on dust-related air quality, limiting the ability for hospitals and emergency services to prepare for potential influxes in patients experiencing cardiovascular and respiratory issues.

In addition to direct consequences to human health, the presence of PM_{coarse} has major implications for plant growth, roadway and pilot visibility, and the Earth's radiative budget. PM_{coarse} decreases agriculture yields due to interference in the stomata and reduction of

photosynthesis (Ahmadzai et al., 2023; Zia-Khan et al., 2015). This not only has economic implications, but it threatens food security. Additionally, airborne dust can reduce visibility, limiting safe transportation. Windblown dust events are estimated to have caused 232 deaths from 2007 to 2017 from highway transportation alone (primarily through visibility reduction), a number previously underestimated due to a lack of dust event data (D. Tong et al., 2023). The subsequent closure of roads due to dust events results in economic losses due to logistical factors such as delays or damage to vehicles (Ardon-Dryer et al., 2023; Ashley et al., 2015; Van Pelt et al., 2020). Unlike fine particulate matter ($PM_{2.5}$; PM with diameters < 2.5 μm) which generally has a cooling effect on the climate, the radiative impact of PM_{coarse} is much more dependent on the background terrain and can produce warming infrared radiative effects (IRE) (Hansen, 2012; Pitari et al., 2015; Saidou Chaibou et al., 2020; Yang et al., 2022). Having a better understanding of this radiative impact is essential in future climate projections (Kok et al., 2023; Leung et al., 2025). However, without robust data, the full scope of dust storm impacts remains uncertain.

Despite limited data availability, the presence of dust is likely increasing over the CONUS with time due to increasing aridity in the Southwest US (Achakulwisut et al., 2019; Ault et al., 2016). Since the pre-industrial era, dust emissions have increased, and in more recent years (1988-2011) there has been an increase in the frequency of dust events (Hooper & Marx, 2018; Leung et al., 2025; D. Q. Tong et al., 2017). Nationally, concentrations of PM_{coarse} and $PM_{2.5}$ from ground monitors have declined due to anthropogenic regulations. However, this downward trend has not been consistent across all regions. In parts of the Southwest and South Central US, dust $PM_{2.5}$ (the fine component of dust) concentrations have increased, particularly during the summer and fall months (Hand et al., 2019). Additionally, the increase in dust storm frequency has likely in turn shortened snow cover duration in the Western US (Painter et al., 2007). In the Great Plains, satellite

observations indicate an increase in coarse-mode aerosols, while ground-based measurements show a rise in PM_{coarse} concentrations in rural regions (Lambert et al., 2020).

Surface measurements are the reference standard for determining surface-level exposure to dust and other PM affecting air quality, but these measurements can be sparse (Figure 2.1). PM_{coarse} is not directly measured, so in order to deduce PM_{coarse}, PM_{10} (PM with diameters < 10 μm) and $PM_{2.5}$ monitors need to be co-located. However, PM_{10} monitors are limited (Figure A.1) and the requirement for colocation further limits the availability of PM_{coarse} observations. As a result, data coverage is often incomplete and varies regionally, allowing for dust storms to occur between monitors. Using the measurements that are available, ground monitor data have been used to evaluate days of elevated PM_{coarse} concentrations and dust $PM_{2.5}$ using speciated data (Hand et al., 2017, 2019; D. Q. Tong et al., 2012). However, ground monitor data is point-specific and does not capture the full extent of dust storms.

Model data, other surface-based observations, and satellite data can also be leveraged to fill in gaps of PM_{coarse} observations to identify and quantify dust. Model data, such as the Modern-Era Retrospective Analysis for Research and Applications, Version 2 (MERRA-2), has multiple dust products such as surface dust concentration and column dust concentration that have been applied to some regions of the world to investigate the frequency and intensity of dust storms and trends in dust concentrations, but these products have not been evaluated or applied to CONUS (Liu, Yin, et al., 2022; Zhu et al., 2025). The National Weather Service (NWS) provides dust-storm data that has been used to investigate dust storms in the US, but it is informed by anecdotal evidence, with events included when observed and reported by individuals such as law enforcement, the media, or the general public and therefore can be incomplete

(https://www.ncdc.noaa.gov/stormevents/faq.jsp) (Ardon-Dryer et al., 2023; Crooks et al., 2016; D. Tong et al., 2023; D. Q. Tong et al., 2022).

Longwave-based satellite data products can detect the presence of dust and provide broader spatial coverage than ground-based observations (Ackerman, 1989). These longwave-based satellite products use the spectral signature of dust in the longwave infrared atmospheric windows (situated in the 8-12 µm spectral band) to identify the presence of dust. Aerosols have a complex refractive index (m) determined through lab analysis to explain the aerosol's absorbing (n) and scattering (k) properties (Equation 1).

$$m = n - ki \qquad \text{Equation 1}$$

Minerals that make up soil such as clays, quartz, and calcite absorb and re-emit terrestrial radiation strongly at ~10 µm but less so at ~12 µm, allowing for the detection of dust (Table 1; Di Biagio et al., 2017). In contrast, water droplets absorb more strongly at ~12 µm than ~10 µm (Table 1; Seinfeld & Pandis, 2016). This difference between the spectral absorption of dust and water provides an opportunity to detect dust using longwave measurements.

Table 1: Complex Refractive Indexes of dust and water droplets at 10.3 µm, 11.2 µm, and 12.3 µm (Di Biagio et al., 2017; Seinfeld & Pandis, 2016)

Wavelength of Radiation	10.3 µm	11.2 µm	12.3 µm
Complex Refractive Index of Dust	1.8 + 0.5i	1.6 + 0.06i	1.5 + 0.04i
Complex Refractive Index of a Cloud (water droplets)	1.2 + 0.06i	1.1 + 0.1i	1.1 + 0.2i

Some satellite data products using this spectral signature to identify the presence of dust are available on web-based platforms available for open-access such as the National Oceanic and Atmospheric Administration (NOAA) Aerosol Detection Product (ADP; Ciren et al., 2024), the dynamic enhancement with background reduction algorithm (DEBRA; Miller et al., 2017), and the European Organization for the Exploitation of Meteorological Satellites (EUMESTAT) Dust RGB (Ackerman, 1997; EUMETSAT, 2023; Fuell et al., 2016; Highwood & Ryder, 2014). These satellite products do not offer information about dust concentration or whether the dust is present at the surface, but they do provide insight into the spatial extent and presence of dust in the atmospheric column.

These satellite products, as well as the reanalysis estimates from MERRA-2 provide a unique opportunity to understand dust/PM_{coarse} events away from surface monitors. However these satellite products have predominantly been used for dust case study analysis, and have not been systematically evaluated for dust quantification over the CONUS (AlNasser & Entekhabi, 2024; Ciren et al., 2024; Miller et al., 2019).

This work evaluates four satellite products and one model reanalysis product against surface concentrations in CONUS to address four primary research questions: (1) Which remote sensing or model product most effectively detects surface-level dust events? (2) What is the probability of dust storms being present in the subregions within CONUS? (3) How large and long-lasting are dust storms in the US? and (4) How many dust storms are identified by ground monitors? In Section 2, we discuss the data products evaluated in this study and present our methods. In Section 3, we evaluate the data products and investigate the dust events in the CONUS and answer our research questions. In Section 4, we discuss our conclusions, limitations of this study, and future work.

CHAPTER 2: METHODS

2.1 Overview

In this analysis, we investigated five products for dust detection in the CONUS. We compared the products to surface ground monitor estimates of PM_{coarse} to identify the product most relevant for surface-level dust. Motivated by air quality concerns in CONUS, we used the Advanced Baseline Imager (ABI) aboard the Geostationary Operational Environmental Satellites-16 (GOES-16) to evaluate satellite data products. GOES-16 provides data over part of the Western Hemisphere having nominal spatial resolution of ~4 km^2 (2 x 2 km pixels) at nadir (0° N, 75.2° W) and temporal resolution of 5-minutes or 10-minutes depending on the product.

2.2 EPA Ground Monitors

We used hourly co-located PM_{10} and $PM_{2.5}$ measurements from EPA FEM/FRM and non FEM/FRM monitors (method codes: 88101, 88502, and 81102) to estimate PM_{coarse} ("coarse mode") concentrations. We chose PM_{coarse} because the total mass of dust particles is predominantly at diameters larger than 2.5 μm (Mahowald et al., 2014). Additionally, using PM_{coarse} will help filter out elevated concentrations of PM due to smoke in the $PM_{2.5}$ fraction of PM_{10} (Silva et al., 1999). For comparison to satellite data, the PM_{coarse} estimates were filtered to measurements where the solar zenith angle is < 80° and the sky is cloud-free directly over the monitor (cloud filtering discussed in section 2.3). The monitors with at least one observation meeting these criteria are shown in Figure 2.1. We evaluated annual and diurnal variability of high PM_{coarse} concentration events through monthly and hourly counts when PM_{coarse} is greater than a certain threshold as described in section 2.3.

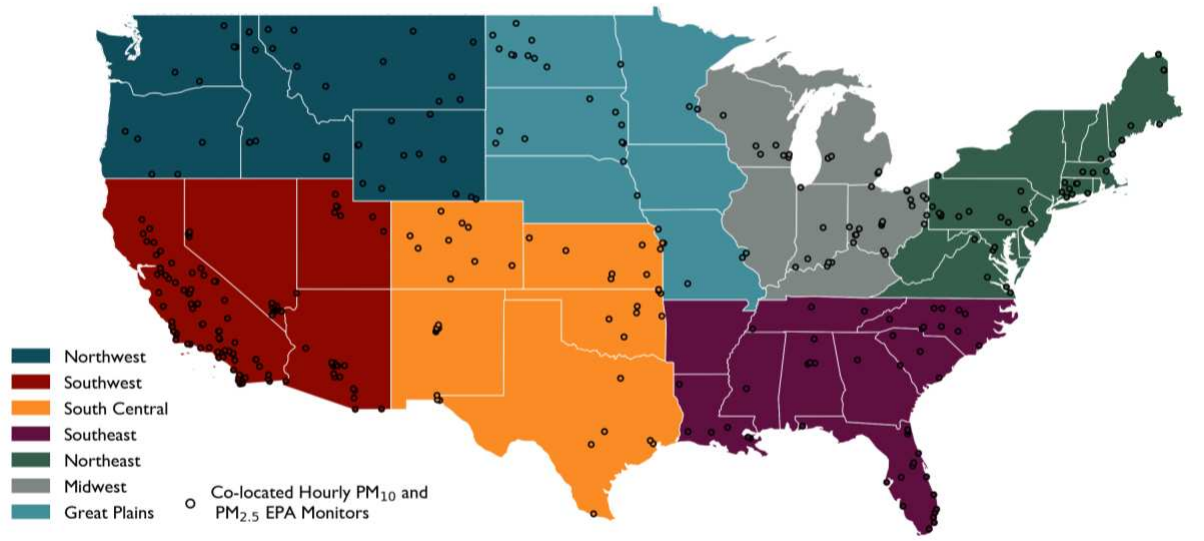

Figure 2.1: US study regions and co-located hourly PM_{10} and $PM_{2.5}$ monitors

2.3 NWS Dust Storms

We used data from the Storm Events Database (SED) by the NOAA NWS to compare with dust storms derived from satellite data products. We used the events labeled "Dust Storm" from the SED. The data comes from a variety of human-reported sources such as county, state, and federal energy officials, law enforcement, insurance industries, the general public, among others (https://www.ncdc.noaa.gov/stormevents/faq.jsp).

2.4 Satellite Products

Four out of the five dust detection products evaluated in this work are satellite products. The satellite products used in this analysis do not necessarily tell us direct information about dust at the surface. However, in this study we focus on evaluating how well they capture surface dust detection by comparing the satellite products to PM_{coarse} estimates, given our primary interest in

surface air quality. The four products we focused on are the NOAA ADP, DEBRA, the pink dust index anomaly (PDI anomaly), and the pink dust index value (PDI value).

1) ADP uses visible reflectance and longwave infrared brightness temperature differences (BTDs) to detect the presence of dust. This product provides a binary identification of smoke and dust at each 10-minute timestep that the algorithm is processed using ABI data (Ciren et al., 2024). For this analysis, we used data quality flags of high, medium, and low.

2) DEBRA is a longwave-based satellite product that provides a confidence factor of the presence of dust (Miller et al., 2017, 2019). This product relies on BTDs, estimates of surface emissivities, and Modern-Era Retrospective Analysis for Research and Applications, Version 2 (MERRA-2) surface temperatures to develop the confidence factor. The algorithm is based on three dust tests using specific channels from the ABI satellite instrument; dust test 1 uses a BTD of the 12.3 and 10.3 μm channels, dust test 2 uses a BTD of the 8.4 and 10.3 μm channels, and dust test 3 uses the BT at 10.3 μm. We used only dust test 1 and 2 and not dust test 3 because through this research, we found dust test 3 to be very similar to dust test 1 but contributed to cloud contamination over the time period and spatial extent we evaluated. The cloud mask used for DEBRA is described in Miller et al. (2017); however, instead of the weighting method described in Miller et al. (2017) where DEBRA was multiplied by the cloud mask, we used a conservative approach and selected only pixels where the cloud mask was 0 (on a scale of 0-1).

3) The PDI anomaly is a longwave-based satellite product calculated using the BTDs of the 12.3 and 10.3 μm channels and 10.3 and 8.4 μm channels, along with the BT of 10.3 μm. This algorithm

uses the same channels as DEBRA but are combined using a method similar to the creation of Dust RGB imagery. This algorithm produces RGB values and then calculates the Euclidean distance from magenta (the color indicating dust) in RGB color space (Knippertz & Stuut, 2014). The anomaly is then created by subtracting the median PDI value from the same hour, month, and year at each pixel (AlNasser & Entekhabi, 2024).

4) As part of this research, we found limitations in the anomaly method when the background PDI was high. This motivated us to also evaluate the absolute PDI value calculated before subtracting the background median value. We used the same cloud mask from DEBRA for the PDI anomaly and value for consistency across the products. The ADP, DEBRA, PDI anomaly and PDI value data products all take advantage of the spectral signature of dust in the longwave to identify its presence.

We also included Aerosol Optical Depth (AOD) in some plots, but we did not directly compare this satellite product to ground measurements. This is because the GOES AOD product is a measure of shortwave light extinction due to particles in the column of atmosphere from the surface to the satellite and therefore can be caused by other aerosols such as smoke, sulfate, and nitrate, not only dust (Laszlo & Liu, 2020). Additionally, the cloud mask used in the AOD algorithm tends to misidentify and filter out optically thick dust plumes as clouds.

2.5 Model Reanalysis Product

In addition to the satellite-derived products above, we evaluated a model-based product for dust identification—the MERRA-2 surface dust concentration. MERRA-2 is an assimilation

product using the Goddard Earth Observing System model and satellite data. This product is available at an hourly temporal resolution and spatial resolution of ~55 x 70 km^2 (Global Modeling and Assimilation Office, 2015). For consistency across products, MERRA-2 data were compared to the same PM_{coarse} observations as the satellite data, namely, cases where the solar zenith angle was < 80° and the sky was cloud-free directly over the surface monitors.

2.6 Evaluation

To evaluate the products, we compared the ADP, DEBRA, PDI anomaly, PDI value, and MERRA-2 surface dust concentration to PM_{coarse} surface estimates for the period 2020-2023. We removed monitors within 10 km of a coast (Great Lakes, Pacific Ocean, and Atlantic Ocean) because these particular satellite algorithms are sensitive to high humidity and certain clouds generally found at coastal regions (AlNasser & Entekhabi, 2024; Miller et al., 2017). Additionally, removing coastal monitors reduced the impact of sea aerosols on PM_{coarse} estimates.

To compare the satellite data products to PM_{coarse} estimates, we used thresholds for the satellite data and monitor data because they are not directly comparable. We determined the thresholds for each product by weighting the precision (Equation 2) and recall (Equation 3) of the products at thresholds ranging from 0-1 for the satellite products and 0-600 µg m^{-3} for the model product and the surface PM_{coarse} estimates.

$$\text{Precision} = \frac{\text{True Positives}}{\text{True Positives} + \text{False Positives}} \qquad \text{Equation 2}$$

$$\text{Recall (or True Positive Rate)} = \frac{\text{True Positives}}{\text{True Positives} + \text{False Negatives}} \qquad \text{Equation 3}$$

In this analysis, given the satellite or model data product identifies dust present at the surface, precision is the proportion of retrievals that are correct based on PM_{coarse} estimates (Equation 2). Given PM_{coarse} is greater than a certain threshold and therefore assuming dust is present at the surface, recall or the true positive rate (TPR) is the proportion of retrievals where the satellite or model data product identifies dust present at the surface (Equation 3). There are cases in which the assumption of dust present at the surface does not hold or elevated PM_{coarse} concentrations are due to non-dust aerosols; however, this assumption is used solely to determine threshold values that optimize the likelihood of success for each product.

To weight precision and recall, we used an F-score (Equation 4). An F-score is an evaluation metric that is not sensitive to our imbalanced dataset, since true negatives comprise the vast majority of our data. The F-score combines precision and recall with a β parameter controlling their relative weight (β>1 minimizes false negatives, β<1 minimizes false positives, and β=1 weights false negatives and false positives equally (Equation 3).

$$F_\beta = \frac{(1+\beta^2) * \text{Precision} * \text{Recall}}{(\beta^2 * \text{Precision}) + \text{Recall}} \qquad \text{Equation 4}$$

We used a beta score of 0.25 instead of the typical value of 1 to weight precision 4x stronger than recall (*Classification*, n.d.; *F1_score*, n.d.; Reddy & R, 2022; Figure A.2). Weighting precision stronger than recall gives us more confidence in the positive values, knowing that there will be elevated surface concentrations caused by dust that the data product is not correctly categorizing. Additionally, a β=1 did not drastically impact the determination of thresholds at high PM_{coarse} observations (Figure A.3). We used the thresholds with the largest F-score unique to each

data product while focusing on higher PM_{coarse} estimates to evaluate each product's true positives, true negatives, false positives, and false negatives.

Similar to the satellite products, we evaluated MERRA-2 surface dust concentration by using the same PM_{coarse} threshold of the best performing satellite product for both the PM_{coarse} estimate and the MERRA-2 surface dust concentration. Additionally, we calculated the Pearson correlation coefficient between the MERRA-2 surface dust concentration and PM_{coarse} estimate.

2.7 Spatiotemporal Analysis

We used the two strongest performing data products and the corresponding satellite thresholds based on the true positive rate to evaluate the spatiotemporal variability in dust in CONUS. As will be shown in section 3.2, these products were the PDI anomaly and PDI value. Pixels with PDI anomalies or PDI values greater than the defined threshold were marked as a positive dust detection. Each positive dust detection corresponded with 5 minutes of dust present– reflecting the temporal resolution of the data product. We filtered out pixels within 20 km of a coast (compared to 10 km in the previous monitor comparison), as the PDI anomaly and PDI values were noticeably more sensitive to the high humidity and low-level coastal clouds not filtered out in the cloud mask. This approach also further reduces the impact from coastal non-dust aerosols, allowing dust to remain the primary contributor to PM_{coarse}. Additionally, we filtered out 13 small desert regions that frequently had a PDI value larger than the threshold that we believe to be due to the surface composition and temperature instead of dust present (Miller et al., 2017) (Figure A.4).

We then compared positive dust detections to surface PM_{coarse} concentrations from 2018-2023 as EPA hourly PM concentration data is not out for 2024 at the time of this study. When we

did not compare the satellite product to surface concentrations, we evaluated positive dust detections from 2018-2024. We proceeded to calculate the probability of dust in a region using the positive dust detections divided by the total number of cloud-free daytime pixels with valid retrievals.

2.8 Clustering: Density-Based Spatial Clustering of Applications with Noise (DBSCAN)

DBSCAN is a type of unsupervised machine learning that clusters data points together and is advantageous for this application as it does not require the number of clusters to be specified beforehand. Additionally, it is able to filter out data as noise if there is not enough surrounding data spatially or temporally. Following previous methods, we applied DBSCAN to the PDI value (AlNasser & Entekhabi, 2024). We chose the PDI value as it had a high true positive rate for the surface comparison and detected more hours of dust present in regions away from monitors than the PDI anomaly. However, this algorithm can be computationally expensive and struggles when the data points vary in density.

Pixels with a PDI value >0.75 were considered a positive dust detection and DBSCAN was applied to the positive dust detections to cluster them into individual dust storms. To be clustered together, positive dust detections were required to be within a certain distance of each other; this distance is called the epsilon value. For this study, we used epsilon values of 25 km spatially and 2 hours temporally to group positive dust detections into clusters. We determined these epsilon values through case study analysis to promote cluster cohesion, avoiding the formation of too many small clusters that should be combined together, while discouraging clusters from different source regions from being clustered together (see Figures A.5 and A.6). The epsilon values had little impact on the total number of pixels clustered (maximum of 1.4% difference; Figure A.7), but

these values significantly impacted the number of clusters created and how the boundaries of an individual dust storm were defined. Additionally, we required at least 10 pixels to be grouped together to be considered a cluster.

Through this analysis, we discovered that some timesteps of the ABI data were corrupted, causing artificially large PDI values. To minimize the impact of corrupted files on the clustering algorithm, we required more than one timestep per cluster. Additionally, we filtered out clusters with an average latitude and longitude within desert regions we found to have anomalously high PDI values due to high surface temperatures (Figure A.4). Meaning, in order for a dust storm from those regions to be counted as a valid dust storm, it must travel beyond the desert long enough that the average latitude and longitude values of the cluster are outside of the bounds of the desert.

Using the clusters, we determined the fractional sizes of dust storms per region and regional exchange of dust storms. For clusters that overlapped regions, we assigned the cluster to the region it was in the most (based on the region where the dust cluster had the highest km^2 hour). Additionally, to compare to other observations, we investigated how often a cluster came within 10 km of at least one monitor, what the surface PM concentrations were when a dust cluster was nearby, and compared the clusters to dust storms reported through the NWS.

CHAPTER 3: RESULTS

3.1 Case Study Day

Figure 3.1 shows the products introduced above in a case study from 17 March 2022, when dust was present over New Mexico, Texas, and northern Mexico. In Figure 3.1a, is the GeoColor (Miller et al., 2020; an approximation of true color imagery for the ABI) imagery from 22:31 UTC. In Figure 3.1b-g, are the satellite and model data products from 22 UTC or averaged across 22 UTC. There were elevated AOD values around the dust storm (Figure 3.1b) but the areas where we would expect the highest AOD values based on the GeoColor imagery were removed by the cloud mask. The MERRA-2 surface dust concentration (Figure 3.1c) was generally elevated but failed to capture the full extent of the dust plumes, particularly the dust plume over New Mexico. This is also true for the MERRA-2 dust AOD (Figure A.8) where there were elevated AOD values over much of Texas but not New Mexico. DEBRA (Figure 3.1d) captured the dust plume over northwestern New Mexico and parts of Texas. However, it failed to capture the full extent of the dust plume, most notably over central Texas where the dust plume is larger than what is identified by DEBRA. Similarly, the ADP (Figure 3.1e) captured the New Mexico plume but failed to capture the other dusty regions. The PDI anomaly (Figure 3.1f) and PDI value (Figure 3.1g) more accurately captured the full extent of the dust plume. However, they also exhibited greater variability, making the distinction between dusty and non-dusty less clear.

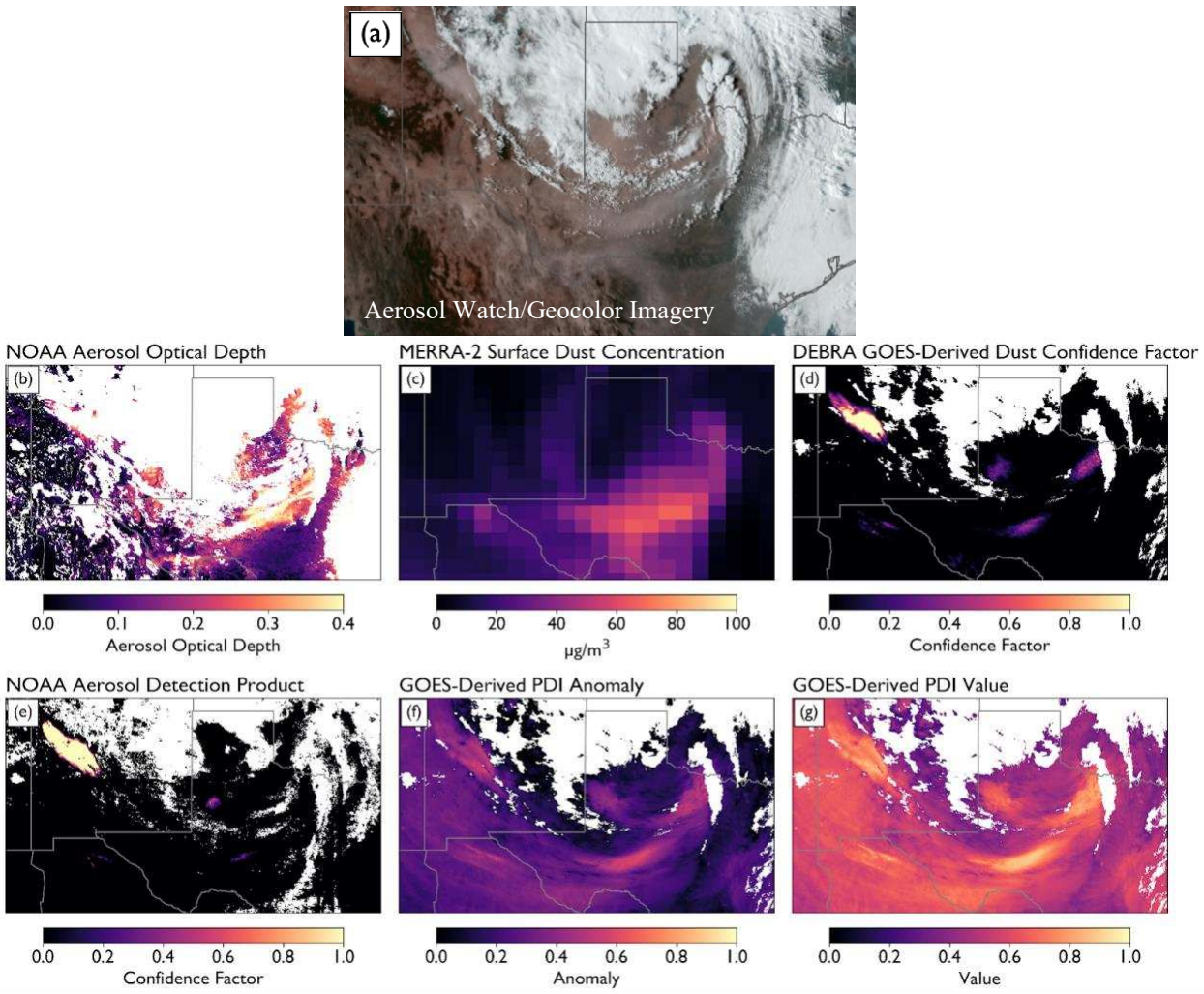

Figure 3.1: Example case study of dust plumes on 17 March 2022. (a) GOES ABI GeoColor imagery at 22:31 UTC showing the dust plumes present over New Mexico, Texas and northern Mexico, (b) NOAA AOD averaged across 22 UTC, (c) Hourly MERRA-2 surface dust concentration from 22:30 UTC, (d-g) hourly averages across 22 UTC, (d) DEBRA confidence factor, (e) NOAA ADP, (f) PDI anomaly, (g) PDI value.

3.2 Evaluation

To evaluate the data products, we identified the thresholds that had the highest F-score while focusing on higher PM_{coarse} concentrations (Figure A.2). Using these thresholds, we investigated true and false positives as well as true and false negatives and TPR (Equation 3) from 2020-2023 (Table 1).

Table 3.1: Number and fraction of retrievals in each category from 2020-2023 (years constrained by the data availability of the EPA monitor data and ADP available on Amazon Web Services).

Data Product and Ground Monitor Thresholds (Data Product / Ground Monitor)	True Negative (Number Fraction)	True Positive (Number Fraction)	False Positive (Number Fraction)	False Negative (Number Fraction)	True Positive Rate
Aerosol Detection Product (ADP) 0.5 / 350 μg m^{-3}	687,165 0.998	22 0.00003	156 0.00023	858 0.00125	0.025
DEBRA 0.55 / 470 μg m^{-3}	1,742,011 0.999	38 0.00002	38 0.00002	917 0.00053	0.040
PDI Anomaly 0.35 / 330 μg m^{-3}	1,738,686 0.999	139 0.00008	49 0.00003	1,699 0.00098	0.076
PDI Value 0.75 / 330 μg m^{-3}	1,738,697 0.999	169 0.00010	38 0.00002	1,669 0.00096	0.092
MERRA-2 Surface Dust Concentration 330 μg m^{-3} / 330 μg m^{-3}	1,741,115 0.999	16 0.000009	49 0.00003	1824 0.00105	0.009

As expected, true negatives dominated the number and fraction of retrievals for all of the data products. The ADP had the lowest TPR at 2.5%. This low TPR could potentially be because the ADP algorithm uses the BTD between the 12 and 11 μm channels rather than between the 12 and 10 μm channels. We expect the BTD between the 12 and 10 μm channels to produce a larger signal of dust present according to the refractive indices from dust samples (Di Biagio et al., 2017). DEBRA had a slightly higher TPR at 4.0% potentially because DEBRA uses the BTD between 12 and 10 μm. Additionally, DEBRA subtracts off a background value that should increase its performance. However, the generally low TPR is likely attributable to a suboptimal background calculation due to coarse resolution of the MERRA-2 skin surface temperature or interannual

variability not accounted for in the emissivity dataset (https://cimss.ssec.wisc.edu/iremis/; Seemann et al., 2008). The PDI anomaly had a higher TPR at 7.6% even while the PM_{coarse} threshold selected for this product was lower than both ADP and DEBRA. Similar to DEBRA, this product subtracts a background value to identify anomalously high values. The PDI value had the highest TPR at 9.2% at the same PM_{coarse} threshold as the PDI anomaly. All true positive retrievals from the PDI value occur in the Southwest and South Central US (Figure A.9). The MERRA-2 surface dust concentration has the lowest TPR at 0.8% and Pearson correlation coefficient equal to 0.17 (Figure A.10). The rest of this analysis will focus on the PDI value and PDI anomaly as they were the strongest performing products.

3.3 Distribution of PM_{coarse} when Satellite Dust Detection is Positive

Figure 3.2 shows the hourly surface PM_{coarse} estimates when there was a positive dust detection from the (a) PDI anomaly and (b) PDI value at the location of the monitors from 2018-2023. The surface concentrations were generally elevated when the PDI value and PDI anomaly were higher than the predetermined thresholds. When the PDI anomaly was greater than 0.35, 85% (220 out of 259) of PM_{coarse} estimates were >180 μg m^{-3}. Similarly, when the PDI value was >0.75, 83% (249 out of 299) of PM_{coarse} estimates were >180 μg m^{-3}. PM_{coarse} estimates <180 μg m^{-3} could indicate false positives of the retrievals or be instances of dust aloft over a monitor. For all other retrievals (PDI anomaly < 0.35 and PDI value < 0.75; Figure 3.2c), only 0.29% of measurements were >180 μg m^{-3}.

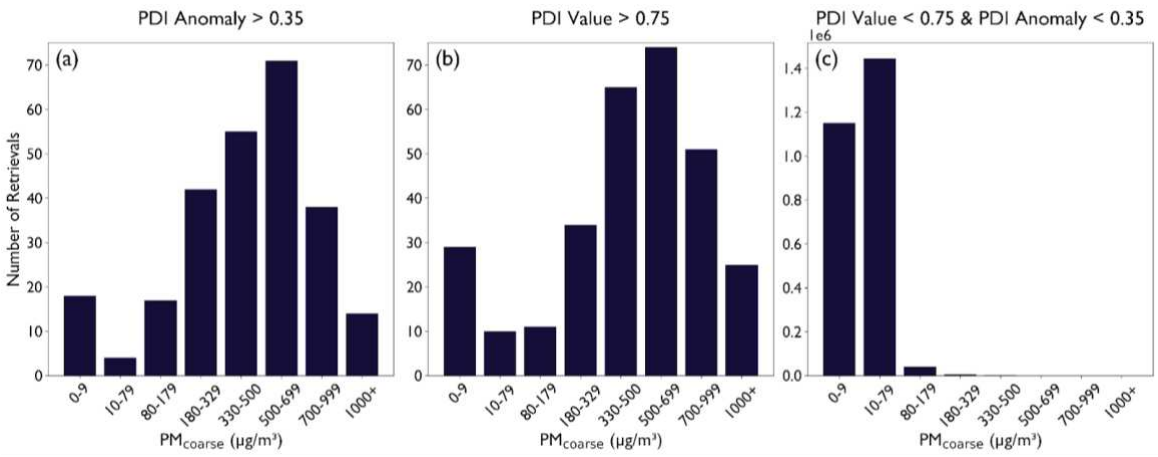

Figure 3.2: Distribution of ground-monitor-observed PM_{coarse} from 2018-2023 when (a) PDI anomaly >0.35, (b) PDI Value >0.75, and (c) PDI anomaly <0.35 and PDI value <0.75.

3.4 Spatial Analysis of PDI Anomalies and PDI Values (2018-2024)

The Southwest and South Central US had the highest number of hours with dust plume present for both data products as shown in Figure 3.3a and 3.3b. The PDI anomaly performed better in the Southwest with a TPR of 10.1% compared to the PDI value TPR of 9.4%. In the South Central, the PDI value had a higher TPR of 5.5% compared to the PDI anomaly TPR of 2.1%. However, monitor density is lower in the South Central, particularly in western and northern Texas where the PDI value detected the highest frequency of dust present with >20 additional hours of dust present compared to the PDI anomaly (Figure 3.3c). The sparse coverage in monitors in those regions makes it difficult to definitively determine which detection method better identifies dust at the surface. Nevertheless, we do know that the anomaly threshold is at an inherent disadvantage in the South Central US due to a high median background PDI, in some cases making it impossible for the PDI anomaly to be >0.35. Potential scaling of the threshold or background PDI could be beneficial for these regions in future research.

The South Central US had the largest number of dust plume hours, dominated by large-scale dust storms persisting multiple hours, known to be predominantly driven by the synoptic

meteorology, expansive source regions, and surface dryness (Robinson & Ardon-Dryer, 2024). The Southwest also experiences frequent dust storms, though these products captured fewer events than expected (Crooks et al., 2016; Hahnenberger & Nicoll, 2012). This was particularly true over Arizona which historically has the largest number of dust storms reported by the NWS (Rublee et al., 2020). Dust events in Arizona are predominantly convection driven and tend to be smaller scale than synoptic driven dust events (Raman et al., 2014). The smaller scale dust storm coupled with higher dew point and relative humidity associated with convective dust storms leads to masking of the dust signal in the longwave, while extensive convective anvil clouds often prevent retrievals altogether (Miller et al., 2019; Robinson & Ardon-Dryer, 2024).

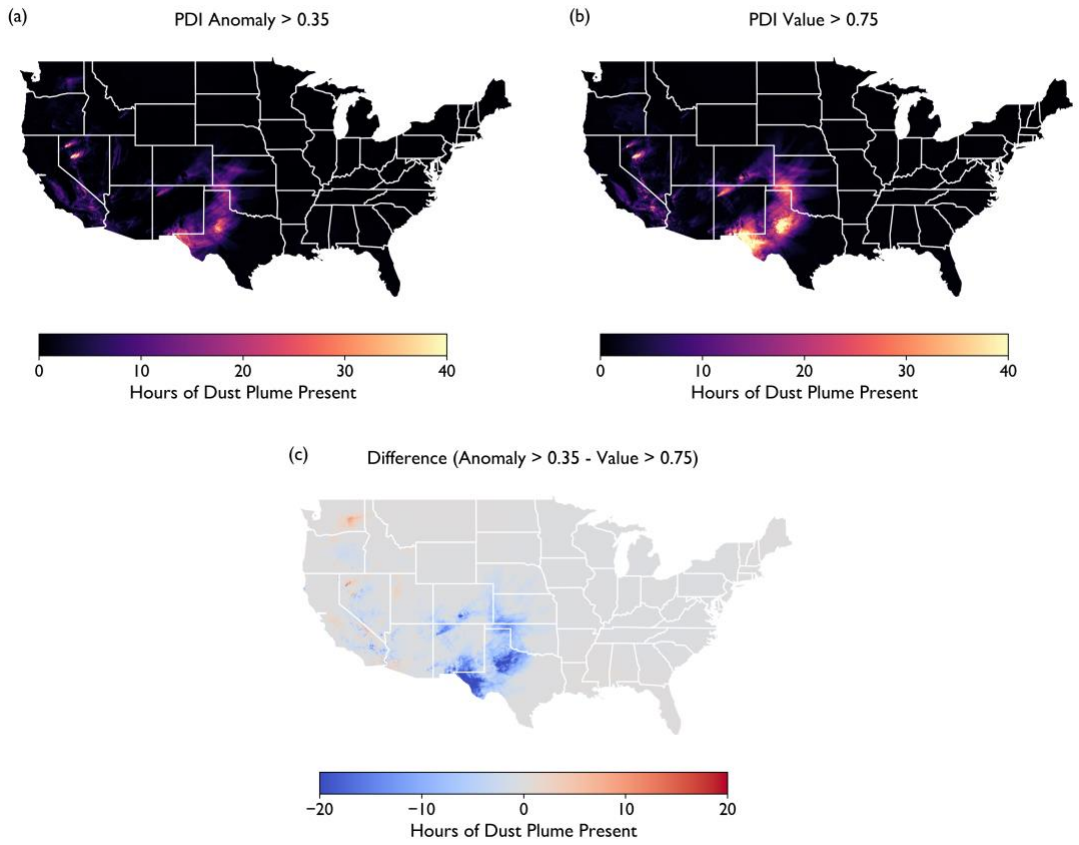

Figure 3.3: Hours of dust plumes present between 2018-2024 over CONUS according to the (a) PDI anomaly, (b) PDI value, and (c) the difference between the PDI anomaly and PDI value.

In the northern Great Plains, PM_{coarse} is present at elevated concentrations, particularly in fall due to agriculture practices (Hand et al., 2017; Lambert et al., 2020). However, these satellite products did not identify many dust events in this region. The lack of dust identification in the Great Plains may be due to the soil composition consisting of smaller concentrations of silicate or not enough soil mass within the column to create a large enough dust signal. Another possibility is a low planetary boundary layer height that is not allowing the dust plume to reach a high enough altitude to be cold enough to create a large enough thermal contrast in the dust infrared-based detection tests.

3.5 Temporal Comparison of Surface Concentrations to PDI Values and Anomalies across the US (2018-2023)

Using the threshold of 330 μg m^{-3} determined in our evaluation, we compared the probability of surface events where PM_{coarse} >330 μg m^{-3} to the probability of dust present from the satellite data. Here we focused on the Southwest, South Central, Great Plains, and Northwest since those are the regions with non-trivial dust present in the PDI values and PDI anomalies shown in Figure 3.4. Across all regions the satellite products had a lower probability of detecting surface dust than the surface monitors, as expected given the low TPRs. Additionally, the increased likelihood of elevated PM_{coarse} estimates may be due to other non-dust sources of PM_{coarse}. However, the PDI value better identifies dust at the surface in some regions than other regions. For example, in April in the South Central US there was a 0.46% probability of PM_{coarse} >330 and a 0.28% probability of dust present at any given location in the region (not only at monitor locations) according to the PDI value.

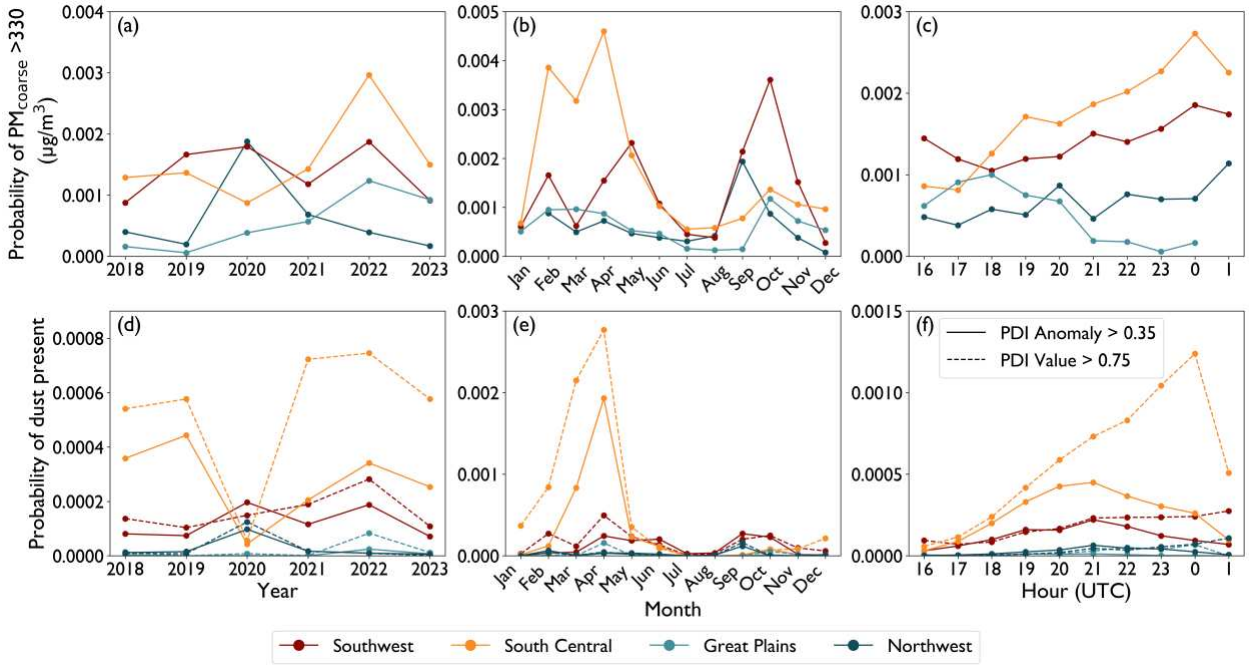

Figure 3.4: Line plots showing the probability of dust present over the CONUS per year (a,d), month (b,e), and hour (c,f), stratified by region. The top row shows the probability of PM_{coarse} >330 µg m^{-3} for the surface monitors, and the bottom row shows the probability using the satellite-based dust products across the entire regions within the US (i.e., not only at the surface monitor locations).

a Southwest

As shown in Figure 3.4a, the annual probabilities of PM_{coarse} estimates exceeding 330 µg m^{-3} at surface monitors were relatively constant over the Southwest US (averaging a 0.14% annual probability of PM_{coarse} >330 µg m^{-3}). The monitor probabilities peaked in spring and fall but we expected to also see a peak in summer that was not observed (Crooks et al., 2016; Hand et al., 2017). The month with the maximum probability of PM_{coarse} >330 µg m^{-3} was October at 0.36% (Figure 3.4b). In the diurnal cycle, there were elevated probabilities of PM_{coarse} exceeding 330 µg m^{-3} at 16 and 17 UTC, followed by a minimum at 18 UTC, and a gradual increase throughout the day (Figure 3.4c). The PDI anomaly and value data were generally consistent with the patterns observed in the monitor data.

The annual probabilities of dust present did not exhibit much variability, averaging 0.012% for the PDI anomaly and 0.016% for the PDI value per year (Figure 3.4d). Both products generally peaked in spring and fall, more noticeably in the PDI value than the PDI anomaly (Figure 3.4e). The probability of dust being present according to the PDI anomaly increases after 16 UTC, peaks at 21 UTC, and decreases the remainder of the day. The diurnal cycle of the PDI value is similar to the diurnal cycle observed by the monitors. At 16 UTC the probability of dust being present according to the PDI value is generally elevated, followed by a minimum at 17 UTC rather than 18 UTC, and a continuous increase throughout the rest of the day (Figure 3.4f).

b South Central

Over the South Central US, the annual probability of PM_{coarse} >330 μg m^{-3} averaged 0.16%, with a minimum in 2020 at 0.09% and maximum in 2022 at 0.3% (Figure 3.4a). The monthly measurement probabilities had a pronounced peak beginning in February and extending into spring with a maximum in April at 0.46% (Figure 3.4b). In the diurnal cycle, the measurement probabilities generally increased throughout the day and peaked at 0 UTC (Figure 3.4c). The probabilities from the satellite data followed similar patterns to the monitor probabilities, with the PDI value having consistently higher probabilities compared to the PDI anomaly. The annual PDI anomaly averaged 0.027% and annual PDI value averaged 0.054% per year (Figure 3.4d). Consistent with the monitor probabilities, both products had a minimum in 2020 potentially due to COVID protocols, changes in meteorology, or natural variability in dust storms (Achakulwisut et al., 2017; Jones et al., 2021; Yaddanapudi & Mishra, 2022). This minimum is more pronounced in the satellite data because the areas with the highest satellite dust probabilities are where there is a lower monitor density.

Similar to the monitor probabilities, the monthly satellite probabilities peaked in spring with a maximum in April (0.19% for PDI anomaly and 0.28% for PDI value) (Figure 3.4e). In April, the monitor probability was less than double the probability of dust present according to the PDI value. However, the South Central TPR was 5.5% for the PDI value data product. Thus, there are likely locations in the South Central US that have a disproportionately large number of elevated PM_{coarse} concentration events that are not detected by surface monitors. Additionally, comparing the relative magnitudes in April, the dust probability in the South Central reached a magnitude 4x higher than that of Southwest while the measurement probability is only 1.5x the magnitude.

The difference in relative magnitudes between South Central and Southwest US is most likely due to the lack of monitors in the South Central leading to an underestimate of the number of events that PM_{coarse} estimates exceed 330 $\mu g\ m^{-3}$. The TPR further supports the lack of monitors causing the differences in relative magnitudes because the TPR in the Southwest was actually higher than the TPR in the South Central US (PDI anomaly: 10.2% compared to 2.1%; PDI value: 9.4% compared to 5.5%). In the diurnal cycle, the probability of dust present according to the PDI anomaly increased throughout the day, peaking at 21 UTC, followed by a steady decrease. The PDI value also increased throughout the day but peaked much later, at 0 UTC, similar to the monitor probabilities (Figure 3.4f).

c Northwest and Great Plains

The Northwest had relatively low probabilities of PM_{coarse} estimates exceeding 330 $\mu g\ m^{-3}$ with 2022 as an exception (Figure 3.4a). We expect the high monitor probability to be partially due to smoke, supported by the corresponding peak in September (Figure 3.4b). However, dust plumes were also in this region during this time, as supported by the peak in PDI anomaly and

value and confirmed through visually examining true color imagery on individual days (Figure 3.4d and 3.4e). The Northwest had a minimal diurnal cycle in the monitor and satellite probabilities (Figure 3.4c and 3.4f). Similarly, the Great Plains had relatively low probabilities of PM_{coarse} estimates exceeding 330 μg m^{-3} but a steady increase throughout the years, peaking in fall and spring (Figure 3.4a and 3.4b). The monitor probabilities peaked earlier in the day (18 UTC), potentially reflective of agricultural practices (Figure 3.4c). The satellite probabilities did not capture the patterns seen in the monitor data, potentially due to the lower concentration of minerals, such as silicate, in the soil (Figure 3.4d - 3.4f). Similar to patterns observed in the Northwest, the probabilities of PM_{coarse} estimates >330 μg m^{-3} in the Great Plains may be influenced by smoke, depending on the conditions and proximity of wildfires.

3.6 DBSCAN

To investigate dust storm duration and size, we applied the clustering algorithm, DBSCAN, to group together pixels where dust was identified as indicated by a PDI value >0.75. We chose the PDI value instead of the PDI anomaly because of the higher TPR in the South Central region, where there are fewer ground monitors. DBSCAN then combines pixels with a positive dust detection (PDI value >0.75) into clusters if the pixels are within 25 km and 2 hours of each other. We used these clusters to investigate information about dust storm duration and size. Figure 3.5 shows an example of the dust storm clustering using the same case study day shown in Figure 3.1, 17 March 2022 from 16 UTC to 0 UTC. In Figure 3.5, there are 6 individual dust clusters. Figure 3.5a presents the dust storms as temporally flattened, while Figure 3.5b shows the clusters' temporal extent.

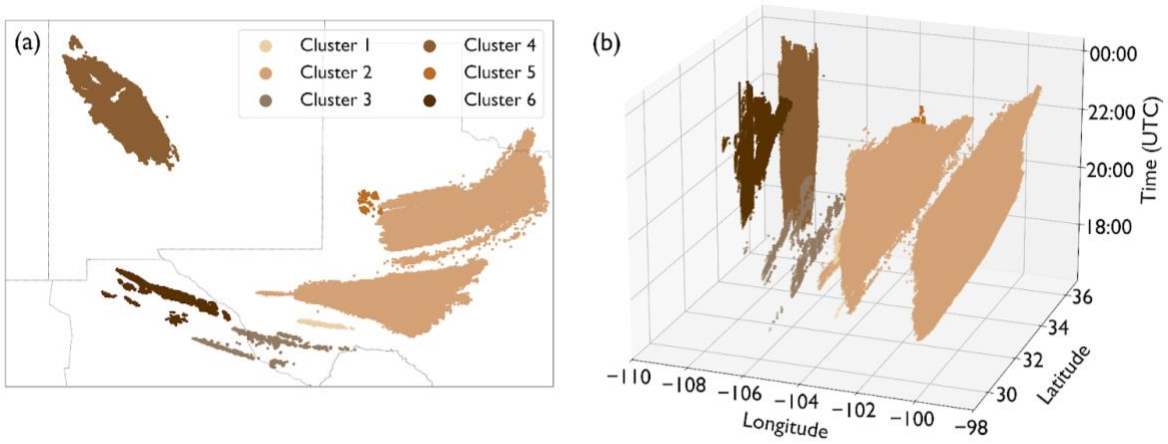

Figure 3.5: Example day of dust clustering showing the evolution of dust plumes over time and space on 17 March 2022 16 UTC - 0 UTC a) temporally flattened dust storms b) 3D dust storms.

a) Dust Cluster Size, Duration, Source Region, and Regional Exchange

Here we will focus on the Southwest and South Central US for dust cluster size and duration as those were the regions with the highest probabilities for dust present (Figure 3.4). As shown in Figure 3.6, there were 887 dust clusters in the South Central and 2,038 dust clusters in the Southwest identified through DBSCAN. While the South Central had fewer dust clusters, when there were dust clusters, they were more likely to be larger and longer-lived than the dust clusters in the Southwest. The greater km^2 hours of dust present in the South Central highlights this. In the Southwest, 0.20% of dust clusters reached 100,000 km^2 hours (4 dust clusters on 4 unique days) and 2.2% reached 10,000 km^2 hours (45 dust clusters on 42 unique days). In the South Central, 3.4% of dust clusters reached 100,000 km^2 hours (30 dust clusters on 29 unique days) and 9.1% of dust clusters reached 10,000 km^2 hours (81 dust clusters on 74 unique days) (Figure 3.6a and 3.6d).

The Southwest had a larger number of hours with dust present than in the South Central (Figure 3.6b and 3.6e); however, when there was a dust cluster, it was more likely to persist longer in the South Central US. Due to the time domain of the satellite data processed, the maximum number of hours present was 10 hours. In the Southwest, 8.7% of dust clusters (177 dust clusters

on 132 unique days) lasted longer than 5 hours. In the South Central, 16% of dust clusters (142 dust clusters on 116 unique days) were present (or lasted) longer than 5 hours. While the Southwest had over 2x as many dust clusters, the combined maximum size of all dust clusters in the Southwest was an order of magnitude smaller than the combined maximum size of dust clusters in the South Central US. In the Southwest, 0.69% of dust clusters reached a maximum size of 10,000 km^2 (14 dust clusters on 13 unique days) and 7.0% reached 1,000 km^2 (142 dust clusters on 107 unique days). In the South Central, 6.0% of dust clusters reached 10,000 km^2 (53 dust clusters on 50 unique days) and 18% reached 1,000 km^2 (158 dust clusters on 121 unique days) (Figure 3.6c and 3.6f).

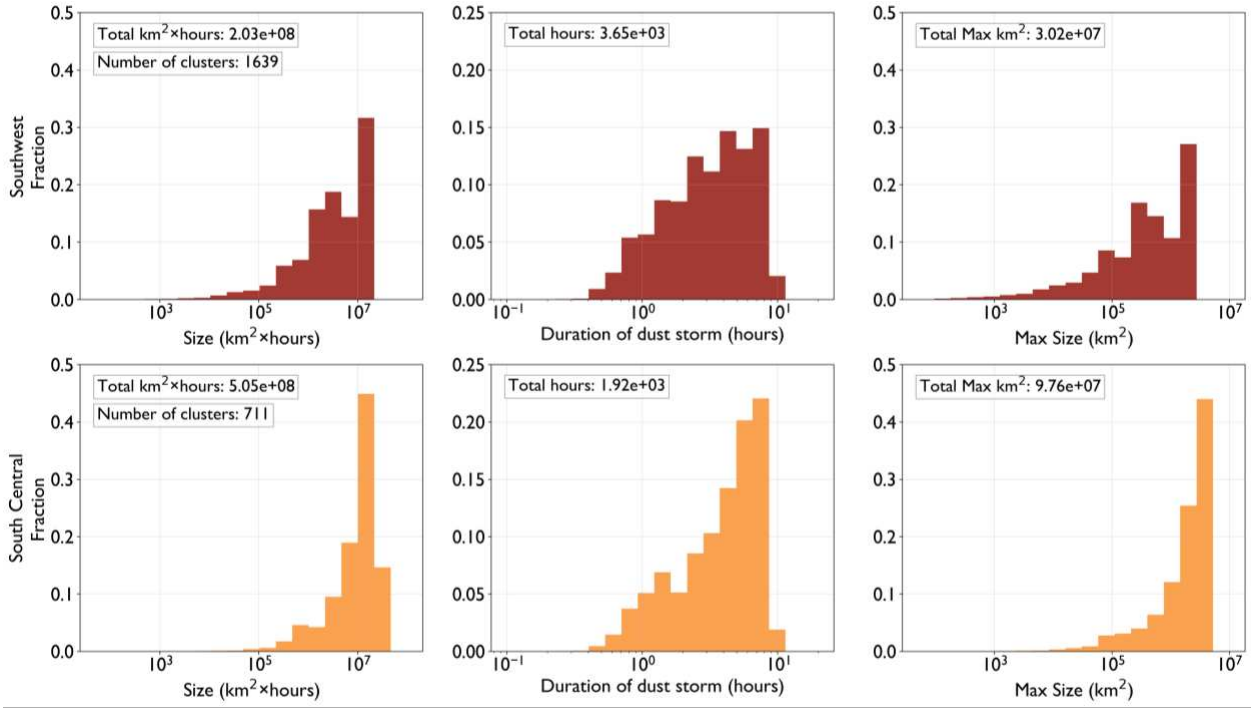

Figure 3.6: Fraction of dust clusters sizes by pixel count in the Southwest and South Central US. The top row shows the dust clusters predominantly in the Southwest (based on km^2 hours) and the bottom row shows the dust clusters predominantly in the South Central. The first column (panels a and d) shows the km^2 hours of the dust clusters. The second column (panels b and e) shows the length of each dust cluster in hours. The third column (panels c and f) shows the cumulative maximum size of the dust clusters in km^2.

Figure 3.7 shows the regional transport of the dust clusters weighted by total pixel count of the dust clusters. For each dust cluster, the source region or regions were identified using the pixel locations at the first timestep of the cluster. Any region the dust cluster contacted at any point in its lifetime was considered a destination region. We then calculated a weighted connection between every source and destination pair for each dust cluster based on the source region's relative contribution to each cluster to determine the transport of the dust storm. We include dust plumes from northern Mexico due to regional transport into the US. The largest transport of dust across regions was from the Chihuahuan Desert in northern Mexico to the South Central US (~6,000,000 dust cluster pixels in the South Central started in northern Mexico). Within the US there was minimal transport between regions.

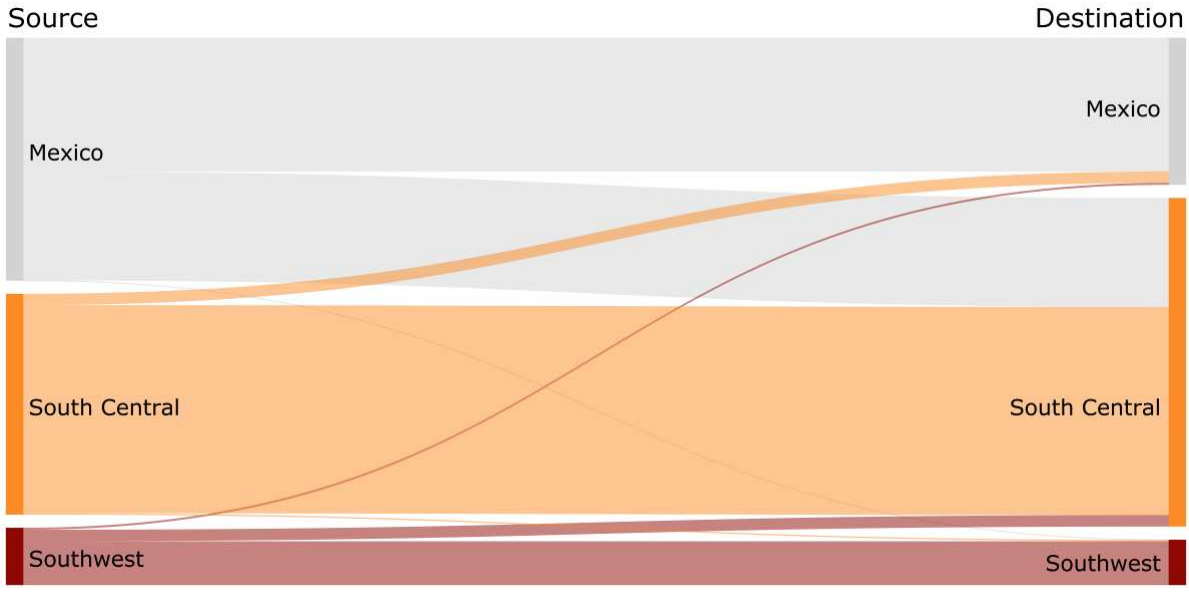

Figure 3.7: Dust cluster source (left) and destination regions (right) connected by the transport of pixels from source region to destination region of the satellite-derived dust clusters.

b) Dust Clusters Comparison to Monitors

To determine the fraction of dust storms identified at ground monitors, we compared the spatial extent of the dust clusters to the locations of ground monitors. In Figure 3.8, we identified the frequency of dust clusters that remained further than 10 km away from co-located hourly PM_{10} and $PM_{2.5}$ monitors from 2018-2023. Of the clusters that entered the Southwest US at any point, 92.4% of clusters (1751 clusters) remained further than 10 km away from co-located PM_{10} and $PM_{2.5}$ monitors. Of the clusters that entered the South Central US at any point, 95.0% of dust clusters (839 clusters) remained further than 10 km away from co-located PM_{10} and $PM_{2.5}$ monitors. When a dust cluster was close to the co-located PM_{10} and $PM_{2.5}$ monitors, there was generally elevated PM_{coarse} compared to PM_{coarse} from the same monitors when a dust cluster was not within 10 km. Applying a 1-tailed z-test to both the Southwest and South Central US, we found that hourly PM_{coarse} estimates were higher when a dust cluster was within 10 km than when a cluster was not within 10 km of the same monitors ($P<.001$ for both Southwest and South Central).

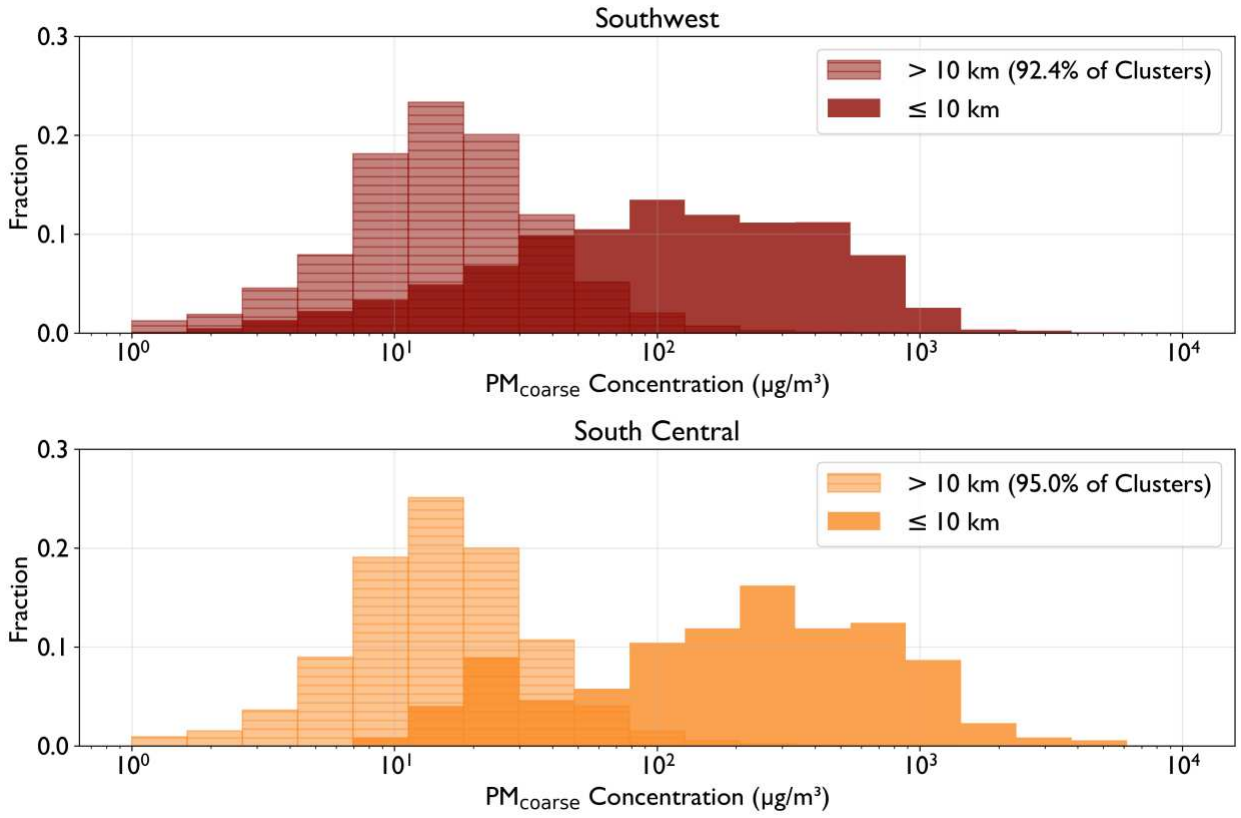

Figure 3.8: Hourly PM_{coarse} estimates at co-located PM_{10} and $PM_{2.5}$ monitors within 10 km of a clustered dust storm (solid bars) compared to hourly PM_{coarse} estimates at the same monitors when a cluster is not within 10 km (hatched bars).

In addition to requiring co-located monitors, we investigated the frequency of a dust cluster being in proximity to individual hourly $PM_{2.5}$ and PM_{10} monitors. In the Southwest US 91.2% (1730) of clusters and in the South Central US 87.5% (773) of clusters remained further than 10 km away from a $PM_{2.5}$ monitor (Figure A.11). In comparison, in the Southwest US, 88.8% (1684) of clusters and in the South Central US 90.6% (800) remained further than 10 km away from a PM_{10} monitor (Figure A.12).

c) Dust clusters comparison with NWS

Here we compare dust clusters to NWS reported dust storms. From 2018-2024, NWS reported 675 county level dust storms. Of the 675 dust storms, there were 67 instances where one county had two dust storms reported on one day. Here we focused only on daily data, resulting in 608 dust storms to compare to the dust clusters. Of the 608 dust storms, there were 110 NWS dust storms where a dust cluster was within ~10 km of the county with a dust storm. These 110 NWS reported dust storms corresponded with 27 dust clusters. Of the 479 NWS reported dust storms without a dust cluster, 324 were in the Southwest, predominantly in Arizona. There were 189 dust clusters >10,000 km^2 hours without a corresponding NWS dust storm reported. Additionally, there were 54 dust storms >10,000 km^2 at their maximum size not reported by the NWS. For example, there were no NWS reported dust storms reported for the case study day in Figures 2 and 6 (17 March 2022). Previous work has also noted missing dust storms from the NWS SED (Ardon-Dryer et al., 2023).

3.7 Quantitatively Estimating the Number of Dust Storms

Focusing on the South Central US, we estimated the number of dust storms missed by the PDI values used in this analysis, by monitor data, and by NWS reported data. In the South Central, the true positive rate of the satellite product used for clustering was 5.5% with a near-zero false positive rate (0.013%). Assuming that the TPR at monitors is applicable throughout the region would mean that only 5.5% of dust storms in the region were captured by the PDI value. Dividing the 887 dust clusters by 5.5% results in ~16,000 total dust clusters in the South Central US from 2018-2024 or ~2,300 dust clusters per year. Incorporating the probabilities of a dust cluster to be further than 10 km from co-located PM_{10} and $PM_{2.5}$ monitors (5.0%) or an NWS reported dust

storm report (3.0%), results in ~2,100 of these "corrected" dust clusters per year are not identified by monitors nor NWS. These estimates are a basic approximation and cannot fully account for uncertainties in the satellite algorithm and clustering methods, but they still provide valuable insight into how many dust storms may go unidentified each year.

CHAPTER 4: CONCLUSIONS

In this study, we evaluated satellite and model data for surface-level dust detection in the CONUS. The products evaluated for dust detection included longwave-based satellite products NOAA ADP, DEBRA, PDI anomaly, and PDI value as well as the model product MERRA-2 surface dust concentration. All dust identification methods evaluated in this study underestimated the frequency of surface dust events when evaluated against PM_{coarse} surface monitor observations. The strongest performing satellite product identified only 9.2% of elevated PM_{coarse} concentration events in the CONUS. Additionally, this satellite product provided the best performance when PM_{coarse} concentrations exceeded 330 $\mu g\ m^{-3}$. Conversely, over 90% of the satellite-observed dust storms occur away from monitoring stations. Given the limited detection performance of satellites and most dust storms occurring away from monitors, this analysis likely captures only the tip of the iceberg regarding dust presence and elevated surface concentrations over the CONUS. Hence, while surface monitors are critical for observing when dust storms occur, our current network is very likely insufficient for detecting many dust storms.

Using the PDI value satellite algorithm coupled with the clustering algorithm, DBSCAN, we identified the largest number of dust events over the Southwest and South Central US. The Southwest US had more frequent dust storms while the South Central US had larger scale (>10,000 km^2) dust storms. Over the Southwest, 0.69% of dust clusters reached a maximum size of 10,000 km^2 (14 dust clusters on 13 unique days) and over the South Central US, 6.0% of dust clusters reached 10,000 km^2 (53 dust clusters on 50 unique days). Additionally, both regions had dust storms that were long-lasting (>5 hours). In the Southwest US, 8.7% of dust events (177 events) lasted longer than 5 hours and in the South Central US, 16% of dust events (142 events) lasted longer than 5 hours.

Our results indicate that there is an under-detection of dust events in CONUS, leading to incomplete exposure estimates, uncertain health risks, and limited public warnings. With the data that is available, prior studies have established the link between dust exposure and adverse health outcomes (Crooks et al., 2016; Rublee et al., 2020; D. Q. Tong et al., 2023). However, without robust data the full extent of the impact of dust on human health is incomplete. Western Texas illustrates this gap in data clearly, with frequent dust storms but few PM_{10} and few co-located PM_{10} and $PM_{2.5}$ monitors. To further investigate dust in this region, we recommend increasing the density of monitors in Texas.

The current lack of ground-based data not only limits our understanding of dust events in the CONUS, it likely hinders the ability of healthcare systems to anticipate and respond to increases in dust-related conditions, such as acute respiratory illnesses including asthma (Kanatani et al., 2010; Rublee et al., 2020). Expanding and enhancing data coverage would also enhance the accuracy and timeliness of public warnings. Notably, many of the dust events identified in this work did not have an NWS dust storm associated, suggesting that the public may not have received official warnings during these events.

4.1 Limitations

The satellite used in this study, GOES-16, is a geostationary satellite positioned over the Western hemisphere, with the first complete year of available data beginning in 2018. To investigate a different temporal or spatial extent than what is evaluated in this study will require a more extensive satellite data record. GOES imagers predating the GOES-16 ABI included some bands at wavelengths used in this study that are useful for dust detection and could potentially be used for historical data. Additionally, due to the nature of this satellite data, observations are

limited to cloud-free, daytime conditions. This poses a challenge for detecting dust storms, as they often are produced by convection and synoptic fronts, which are frequently accompanied with cloud cover, and they may occur at night.

In addition to the general limitations of GOES-16, the PDI value algorithm has additional constraints. As noted in the study, desert regions can produce false positives; however, these areas were typically spatially limited and were largely masked in our analysis. Furthermore, the satellite-based dust detection algorithms failed to capture dust in regions where it was expected. For example, in the Great Plains, an area with agricultural activity known to generate dust, few dust plumes were detected, even during periods of elevated PM_{coarse} observations.

In evaluating the satellite and model products, we were constrained to only locations where ground monitors were present. However, through this work we identified locations where there were frequent dust storms where no ground monitors were present, notably in western Texas. Without ground measurements it is challenging to assess the true performance of the satellite product in this area. Additionally, evaluating the data products against PM_{coarse} observations may underestimate the performance of the data products due to contributions from non-dust aerosols like sea salt.

4.2 Future work

This work is the first in the United States to aggregate satellite-identified dust observations into spatiotemporal representations of dust events. This data provides valuable insight into the frequency, size, and duration of dust storms in CONUS. Here we explored this data relative to ground monitors and NWS dust storms. There are multiple additional applications of the dust events data such as assessing health outcomes, examining traffic accidents due to wind-blown dust,

and improving dust storm warning systems. Comparing the dust data to emergency department visits or rates of mortality, cardiovascular, and respiratory disease can further enhance our understanding of the human health outcomes associated with dust exposure. Additionally, comparing the dust clusters to roadway data could provide further insight into the frequency and severity of wind-blown dust fatalities and accidents. Finally, using satellite data for early detection of a dust storm can provide earlier warnings downwind.

This work focused on algorithms already produced which predominantly used longwave data. Incorporating shortwave data into the longwave-based algorithm should enhance the ability to differentiate dust events from clouds and deserts. Shortwave data can be incorporated using the channels available on GOES or by integrating the Tropospheric Emissions: Monitoring Pollution (TEMPO) satellite, which offers a wider range of shortwave channels.

This work uses the clustering algorithm DBSCAN, following previous literature, but the chosen parameters greatly impact how individual dust storms were categorized (AlNasser & Entekhabi, 2024). A similar clustering algorithm, the hierarchical density-based clustering of applications with noise (HDBSCAN), can more effectively handle data points of varying densities and would be beneficial to investigate further. Additionally, it can identify potential subclusters within a cluster, which may aid in more intuitively attributing sources of a dust plume. Through this research, we identified the need for more PM_{coarse} observations in the US. One approach for addressing this gap is to deploy additional EPA monitors or improve low-cost sensors for accurate PM_{coarse} measurements to increase spatial coverage.

REFERENCES

Achakulwisut, P., Anenberg, S. C., Neumann, J. E., Penn, S. L., Weiss, N., Crimmins, A., Fann, N., Martinich, J., Roman, H., & Mickley, L. J. (2019). Effects of Increasing Aridity on Ambient Dust and Public Health in the U.S. Southwest Under Climate Change. *GeoHealth*, *3*(5), 127–144. https://doi.org/10.1029/2019GH000187

Achakulwisut, P., Shen, L., & Mickley, L. J. (2017). What Controls Springtime Fine Dust Variability in the Western United States? Investigating the 2002–2015 Increase in Fine Dust in the U.S. Southwest. *Journal of Geophysical Research: Atmospheres*, *122*(22). https://doi.org/10.1002/2017JD027208

Ackerman, S. A. (1989). Using the radiative temperature difference at 3.7 and 11 μm to tract dust outbreaks. *Remote Sensing of Environment*, *27*(2), 129–133. https://doi.org/10.1016/0034-4257(89)90012-6

Ackerman, S. A. (1997). Remote sensing aerosols using satellite infrared observations. *Journal of Geophysical Research: Atmospheres*, *102*(D14), 17069–17079. https://doi.org/10.1029/96JD03066

Ahmadzai, H., Malhotra, A., & Tutundjian, S. (2023). Assessing the impact of sand and dust storm on agriculture: Empirical evidence from Mongolia. *PLOS ONE*, *18*(2), e0269271. https://doi.org/10.1371/journal.pone.0269271

AlNasser, F., & Entekhabi, D. (2024). DustSCAN: A Five Year (2018-2022) Hourly Dataset of Dust Plumes From SEVIRI. *Scientific Data*, *11*(1), 607. https://doi.org/10.1038/s41597-024-03452-4

Ardon-Dryer, K., Gill, T. E., & Tong, D. Q. (2023). When a Dust Storm Is Not a Dust Storm: Reliability of Dust Records From the Storm Events Database and Implications for Geohealth Applications. *GeoHealth*, *7*(1), e2022GH000699. https://doi.org/10.1029/2022GH000699

Ashley, W. S., Strader, S., Dziubla, D. C., & Haberlie, A. (2015). *Driving Blind: Weather-Related Vision Hazards and Fatal Motor Vehicle Crashes*. https://doi.org/10.1175/BAMS-D-14-00026.1

Ault, T. R., Mankin, J. S., Cook, B. I., & Smerdon, J. E. (2016). Relative impacts of mitigation, temperature, and precipitation on 21st-century megadrought risk in the American Southwest. *Science Advances*, *2*(10), e1600873. https://doi.org/10.1126/sciadv.1600873

Chen, R., Yin, P., Meng, X., Wang, L., Liu, C., Niu, Y., Liu, Y., Liu, J., Qi, J., You, J., Kan, H., & Zhou, M. (2019). Associations between Coarse Particulate Matter Air Pollution and Cause-Specific Mortality: A Nationwide Analysis in 272 Chinese Cities. *Environmental Health Perspectives*, *127*(1), 017008. https://doi.org/10.1289/EHP2711

Ciren, P., Kondragunta, S., & Huff, A. (2024). *ABI Enterprise Processing System Aerosol Detection Product*.

Classification: Accuracy, recall, precision, and related metrics | Machine Learning. (n.d.). Google for Developers. Retrieved July 15, 2025, from https://developers.google.com/machine-learning/crash-course/classification/accuracy-precision-recall

Crooks, J. L., Cascio, W. E., Percy, M. S., Reyes, J., Neas, L. M., & Hilborn, E. D. (2016). The Association between Dust Storms and Daily Non-Accidental Mortality in the United

States, 1993-2005. *Environmental Health Perspectives*, *124*(11), 1735–1743. https://doi.org/10.1289/EHP216

Di Biagio, C., Formenti, P., Balkanski, Y., Caponi, L., Cazaunau, M., Pangui, E., Journet, E., Nowak, S., Caquineau, S., Andreae, M. O., Kandler, K., Saeed, T., Piketh, S., Seibert, D., Williams, E., & Doussin, J.-F. (2017). Global scale variability of the mineral dust long-wave refractive index: A new dataset of in situ measurements for climate modeling and remote sensing. *Atmospheric Chemistry and Physics*, *17*(3), 1901–1929. https://doi.org/10.5194/acp-17-1901-2017

EUMETSAT. (2023). *Dust RGB Quick Guide*. EUMETSAT. https://user.eumetsat.int/resources/user-guides/dust-rgb-quick-guide

F1_score. (n.d.). Scikit-Learn. Retrieved July 15, 2025, from https://scikit-learn/stable/modules/generated/sklearn.metrics.f1_score.html

Fischer, E. V., Hsu, N. C., Jaffe, D. A., Jeong, M.-J., & Gong, S. L. (2009). A decade of dust: Asian dust and springtime aerosol load in the U.S. Pacific Northwest. *Geophysical Research Letters*, *36*(3). https://doi.org/10.1029/2008GL036467

Fuell, K., Guyer, B., Kann, D., Molthan, A., & Elmer, N. (2016). Next generation satellite RGB dust imagery leads to op-erational changes at NWS Alburquerque. *Journal of Operational Meteorology*, *04*(06), 75–91. https://doi.org/10.15191/nwajom.2016.0406

Global Modeling and Assimilation Office (GMAO). (2015). *MERRA-2 tavg1_2d_aer_Nx: 2d,1-Hourly,Time-averaged,Single-Level,Assimilation,Aerosol Diagnostics V5.12.4, Greenbelt, MD, USA, Goddard Earth Sciences Data and Information Services Center (GES DISC)*.

Guzman-Gonzalez, J., Fitzgerald, R. M., Karle, N. N., Sakai, R. K., & Stockwell, W. R. (2024). Particulate Matter in the American Southwest: Detection and Analysis of Dust Storms Using Surface Measurements and Ground-Based LIDAR. *Atmosphere*, *15*(1), 110. https://doi.org/10.3390/atmos15010110

Hahnenberger, M., & Nicoll, K. (2012). Meteorological characteristics of dust storm events in the eastern Great Basin of Utah, U.S.A. *Atmospheric Environment*, *60*, 601–612. https://doi.org/10.1016/j.atmosenv.2012.06.029

Hand, J. L., Gill, T. E., & Schichtel, B. A. (2017). Spatial and seasonal variability in fine mineral dust and coarse aerosol mass at remote sites across the United States. *Journal of Geophysical Research: Atmospheres*, *122*(5), 3080–3097. https://doi.org/10.1002/2016JD026290

Hand, J. L., Gill, T. E., & Schichtel, B. A. (2019). Urban and rural coarse aerosol mass across the United States: Spatial and seasonal variability and long-term trends. *Atmospheric Environment*, *218*, 117025. https://doi.org/10.1016/j.atmosenv.2019.117025

Hansen, K. (2012). *Dust's warming counters half of its cooling effect*. NASA Global Climate Change: Vital Signs of the Planet. https://climate.nasa.gov/news/807/dusts-warming-counters-half-of-its-cooling-effect

Highwood, E. J., & Ryder, C. L. (2014). Radiative Effects of Dust. In P. Knippertz & J.-B. W. Stuut (Eds.), *Mineral Dust: A Key Player in the Earth System* (pp. 267–286). Springer Netherlands. https://doi.org/10.1007/978-94-017-8978-3_11

Hooper, J., & Marx, S. (2018). A global doubling of dust emissions during the Anthropocene? *Global and Planetary Change*, *169*, 70–91. https://doi.org/10.1016/j.gloplacha.2018.07.003

Jones, D., Klose, D. S., Keeling, W., & Kaase, D. G. (2021). *Analyzing the Impact of COVID-19 on Texas High Plains Agriculture*. *19*(1).

Kanatani, K. T., Ito, I., Al-Delaimy, W. K., Adachi, Y., Mathews, W. C., & Ramsdell, J. W. (2010). Desert Dust Exposure Is Associated with Increased Risk of Asthma Hospitalization in Children. *American Journal of Respiratory and Critical Care Medicine*, *182*(12), 1475–1481. https://doi.org/10.1164/rccm.201002-0296OC

Knippertz, P., & Stuut, J.-B. W. (Eds.). (2014). *Mineral Dust: A Key Player in the Earth System*. Springer Netherlands. https://doi.org/10.1007/978-94-017-8978-3

Kodros, J. K., Volckens, J., Jathar, S. H., & Pierce, J. R. (2018). Ambient Particulate Matter Size Distributions Drive Regional and Global Variability in Particle Deposition in the Respiratory Tract. *GeoHealth*, *2*(10), 298–312. https://doi.org/10.1029/2018GH000145

Kok, J. F., Storelvmo, T., Karydis, V. A., Adebiyi, A. A., Mahowald, N. M., Evan, A. T., He, C., & Leung, D. M. (2023). Mineral dust aerosol impacts on global climate and climate change. *Nature Reviews Earth & Environment*, *4*(2), 71–86. https://doi.org/10.1038/s43017-022-00379-5

Kumar, P., Hopke, P. K., Raja, S., Casuccio, G., Lersch, T. L., & West, R. R. (2012). Characterization and heterogeneity of coarse particles across an urban area. *Atmospheric Environment*, *46*, 449–459. https://doi.org/10.1016/j.atmosenv.2011.09.018

Lambert, A., Hallar, A. G., Garcia, M., Strong, C., Andrews, E., & Hand, J. L. (2020). Dust Impacts of Rapid Agricultural Expansion on the Great Plains. *Geophysical Research Letters*, *47*(20), e2020GL090347. https://doi.org/10.1029/2020GL090347

Laszlo, I., & Liu, H. (2020). *EPS Aerosol Optical Depth (AOD) Algorithm Theoretical Basis Document*.

Leung, D. M., Kok, J. F., Li, L., Lawrence, D. M., Mahowald, N. M., Tilmes, S., & Kluzek, E. (2025). A global dust emission dataset for estimating dust radiative forcings in climate models. *Atmospheric Chemistry and Physics*, *25*(4), 2311–2331. https://doi.org/10.5194/acp-25-2311-2025

Liu, C., Cai, J., Chen, R., Sera, F., Guo, Y., Tong, S., Li, S., Lavigne, E., Correa, P. M., Ortega, N. V., Orru, H., Maasikmets, M., Jaakkola, J. J. K., Ryti, N., Breitner, S., Schneider, A., Katsouyanni, K., Samoli, E., Hashizume, M., … Kan, H. (2022). Coarse Particulate Air Pollution and Daily Mortality: A Global Study in 205 Cities. *American Journal of Respiratory and Critical Care Medicine*, *206*(8), 999–1007. https://doi.org/10.1164/rccm.202111-2657OC

Liu, C., Yin, Z., He, Y., & Wang, L. (2022). Climatology of Dust Aerosols over the Jianghan Plain Revealed with Space-Borne Instruments and MERRA-2 Reanalysis Data during 2006–2021. *Remote Sensing*, *14*(17), Article 17. https://doi.org/10.3390/rs14174414

Mahowald, N., Albani, S., Kok, J. F., Engelstaeder, S., Scanza, R., Ward, D. S., & Flanner, M. G. (2014). The size distribution of desert dust aerosols and its impact on the Earth system. *Aeolian Research*, *15*, 53–71. https://doi.org/10.1016/j.aeolia.2013.09.002

Malm, W. C., & Hand, J. L. (2007). An examination of the physical and optical properties of aerosols collected in the IMPROVE program. *Atmospheric Environment*, *41*(16), 3407–3427. https://doi.org/10.1016/j.atmosenv.2006.12.012

Malm, W. C., Pitchford, M. L., McDade, C., & Ashbaugh, L. L. (2007). Coarse particle speciation at selected locations in the rural continental United States. *Atmospheric Environment*, *41*(10), 2225–2239. https://doi.org/10.1016/j.atmosenv.2006.10.077

Masri, S., Kang, C.-M., & Koutrakis, P. (2015). Composition and Sources of Fine and Coarse Particles Collected during 2002–2010 in Boston, MA. *Journal of the Air & Waste Management Association (1995)*, *65*(3), 287–297. https://doi.org/10.1080/10962247.2014.982307

Miller, S. D., Bankert, R. L., Solbrig, J. E., Forsythe, J. M., Noh, Y.-J., & Grasso, L. D. (2017). A Dynamic Enhancement With Background Reduction Algorithm: Overview and Application to Satellite-Based Dust Storm Detection. *Journal of Geophysical Research: Atmospheres*, *122*(23), 12,938-12,959. https://doi.org/10.1002/2017JD027365

Miller, S. D., Grasso, L., Bian, Q., Kreidenweis, S., Dostalek, J., Solbrig, J., Bukowski, J., Van Den Heever, S. C., Wang, Y., Xu, X., Wang, J., Walker, A., Wu, T.-C., Zupanski, M., Chiu, C., & Reid, J. (2019). *<i>A Tale of Two Dust Storms</i>: Analysis of a Complex Dust Event in the Middle East* [Preprint]. Aerosols/Remote Sensing/Data Processing and Information Retrieval. https://doi.org/10.5194/amt-2019-82

Miller, S. D., Lindsey, D. T., Seaman, C. J., & Solbrig, J. E. (2020). *GeoColor: A Blending Technique for Satellite Imagery*. https://doi.org/10.1175/JTECH-D-19-0134.1

Painter, T. H., Barrett, A. P., Landry, C. C., Neff, J. C., Cassidy, M. P., Lawrence, C. R., McBride, K. E., & Farmer, G. L. (2007). Impact of disturbed desert soils on duration of mountain snow cover. *Geophysical Research Letters*, *34*(12). https://doi.org/10.1029/2007GL030284

Perry, K. D., Cahill, T. A., Eldred, R. A., Dutcher, D. D., & Gill, T. E. (1997). Long-range transport of North African dust to the eastern United States. *Journal of Geophysical Research: Atmospheres*, *102*(D10), 11225–11238. https://doi.org/10.1029/97JD00260

Pitari, G., Di Genova, G., Coppari, E., De Luca, N., Di Carlo, P., Iarlori, M., & Rizi, V. (2015). Desert dust transported over Europe: Lidar observations and model evaluation of the radiative impact. *Journal of Geophysical Research: Atmospheres*, *120*(7), 2881–2898. https://doi.org/10.1002/2014JD022875

Prospero, J. M. (1999a). Long-range transport of mineral dust in the global atmosphere: Impact of African dust on the environment of the southeastern United States. *Proceedings of the National Academy of Sciences*, *96*(7), 3396–3403. https://doi.org/10.1073/pnas.96.7.3396

Prospero, J. M. (1999b). Long-range transport of mineral dust in the global atmosphere: Impact of African dust on the environment of the southeastern United States. *Proceedings of the National Academy of Sciences*, *96*(7), 3396–3403. https://doi.org/10.1073/pnas.96.7.3396

Prospero, J. M., Blades, E., Mathison, G., & Naidu, R. (2005). Interhemispheric transport of viable fungi and bacteria from Africa to the Caribbean with soil dust. *Aerobiologia*, *21*(1), 1–19. https://doi.org/10.1007/s10453-004-5872-7

Raman, A., Arellano, A. F., & Brost, J. J. (2014). Revisiting haboobs in the southwestern United States: An observational case study of the 5 July 2011 Phoenix dust storm. *Atmospheric Environment*, *89*, 179–188. https://doi.org/10.1016/j.atmosenv.2014.02.026

Reddy, B. H., & R, K. P. (2022). Classification of Fire and Smoke Images using Decision Tree Algorithm in Comparison with Logistic Regression to Measure Accuracy, Precision, Recall, F-score. *2022 14th International Conference on Mathematics, Actuarial Science, Computer Science and Statistics (MACS)*, 1–5. https://doi.org/10.1109/MACS56771.2022.10022449

Robinson, M. C., & Ardon-Dryer, K. (2024). Characterization of 21 years of dust events across four West Texas regions. *Aeolian Research*, *67–69*, 100930. https://doi.org/10.1016/j.aeolia.2024.100930

Rublee, C. S., Sorensen, C. J., Lemery, J., Wade, T. J., Sams, E. A., Hilborn, E. D., & Crooks, J. L. (2020). Associations Between Dust Storms and Intensive Care Unit Admissions in the United States, 2000–2015. *GeoHealth*, *4*(8), e2020GH000260. https://doi.org/10.1029/2020GH000260

Saidou Chaibou, A. A., Ma, X., & Sha, T. (2020). Dust radiative forcing and its impact on surface energy budget over West Africa. *Scientific Reports*, *10*(1), 12236. https://doi.org/10.1038/s41598-020-69223-4

Seemann, S. W., Borbas, E. E., Knuteson, R. O., Stephenson, G. R., & Huang, H.-L. (2008). *Development of a Global Infrared Land Surface Emissivity Database for Application to Clear Sky Sounding Retrievals from Multispectral Satellite Radiance Measurements*. https://doi.org/10.1175/2007JAMC1590.1

Seinfeld, J. H., & Pandis, S. N. (2016). *Atmospheric Chemistry and Physics: From Air Pollution to Climate Change.*

Silva, P. J., Liu, D.-Y., Noble, C. A., & Prather, K. A. (1999). Size and Chemical Characterization of Individual Particles Resulting from Biomass Burning of Local Southern California Species. *Environmental Science & Technology*, *33*(18), 3068–3076. https://doi.org/10.1021/es980544p

Sprigg, W. A., Gill, T. E., Tong, D. Q., Li, J., Ren, L., & Van Pelt, R. S. (2022). Are Opportunities to Apply Airborne Dust Research Being Missed? *Bulletin of the American*

Meteorological Society, *103*(6), E1587–E1594. https://doi.org/10.1175/BAMS-D-22-0034.1

Tong, D., Feng, I., Gill, T. E., Schepanski, K., & Wang, J. (2023). How Many People Were Killed by Windblown Dust Events in the United States? *Bulletin of the American Meteorological Society*, *104*(5), E1067–E1084. https://doi.org/10.1175/BAMS-D-22-0186.1

Tong, D. Q., Dan, M., Wang, T., & Lee, P. (2012). Long-term dust climatology in the western United States reconstructed from routine aerosol ground monitoring. *Atmospheric Chemistry and Physics*, *12*(11), 5189–5205. https://doi.org/10.5194/acp-12-5189-2012

Tong, D. Q., Gill, T. E., Sprigg, W. A., Van Pelt, R. S., Baklanov, A. A., Barker, B. M., Bell, J. E., Castillo, J., Gassó, S., Gaston, C. J., Griffin, D. W., Huneeus, N., Kahn, R. A., Kuciauskas, A. P., Ladino, L. A., Li, J., Mayol-Bracero, O. L., McCotter, O. Z., Méndez-Lázaro, P. A., … Vimic, A. V. (2023). Health and Safety Effects of Airborne Soil Dust in the Americas and Beyond. *Reviews of Geophysics*, *61*(2), e2021RG000763. https://doi.org/10.1029/2021RG000763

Tong, D. Q., Gorris, M. E., Gill, T. E., Ardon-Dryer, K., Wang, J., & Ren, L. (2022). Dust Storms, Valley Fever, and Public Awareness. *GeoHealth*, *6*(8), e2022GH000642. https://doi.org/10.1029/2022GH000642

Tong, D. Q., Wang, J. X. L., Gill, T. E., Lei, H., & Wang, B. (2017). Intensified dust storm activity and Valley fever infection in the southwestern United States. *Geophysical Research Letters*, *44*(9), 4304–4312. https://doi.org/10.1002/2017GL073524

Van Pelt, R. S., Tatarko, J., Gill, T. E., Chang, C., Li, J., Eibedingil, I. G., & Mendez, M. (2020). Dust emission source characterization for visibility hazard assessment on Lordsburg

Playa in Southwestern New Mexico, USA. *Geoenvironmental Disasters*, *7*(1), 34. https://doi.org/10.1186/s40677-020-00171-x

Yaddanapudi, R., & Mishra, A. K. (2022). Compound impact of drought and COVID-19 on agriculture yield in the USA. *Science of The Total Environment*, *807*, 150801. https://doi.org/10.1016/j.scitotenv.2021.150801

Yang, D., Zhang, H., Wang, Z., Zhao, S., & Li, J. (2022). Changes in anthropogenic particulate matters and resulting global climate effects since the Industrial Revolution. *International Journal of Climatology*, *42*(1), 315–330. https://doi.org/10.1002/joc.7245

Zhu, Q., Liu, Y., & Xiao, N. (2025). *The Frequency and Intensity of Extreme Dust Events and Related Driving Factors in Major Dust Sources Based on MERRA-2 Aerosol Reanalysis*. https://doi.org/10.1175/JCLI-D-24-0702.1

Zia-Khan, S., Spreer, W., Pengnian, Y., Zhao, X., Othmanli, H., He, X., & Müller, J. (2015). Effect of Dust Deposition on Stomatal Conductance and Leaf Temperature of Cotton in Northwest China. *Water*, *7*(1), Article 1. https://doi.org/10.3390/w7010116

APPENDIX: SUPPLEMENTAL FIGURES

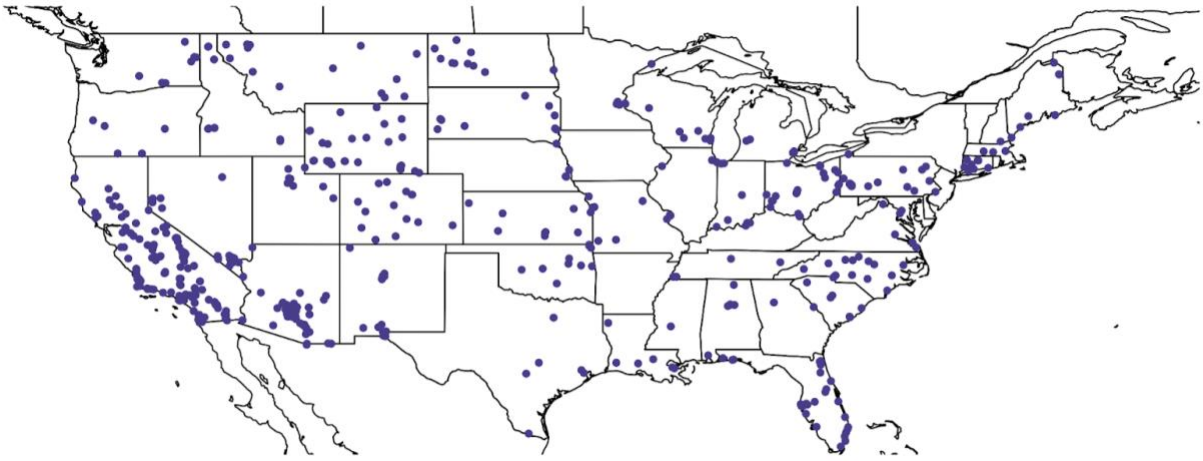

Figure A.1: Locations of hourly EPA PM_{10} monitors with a measurement from 2018-2023 in the contiguous US.

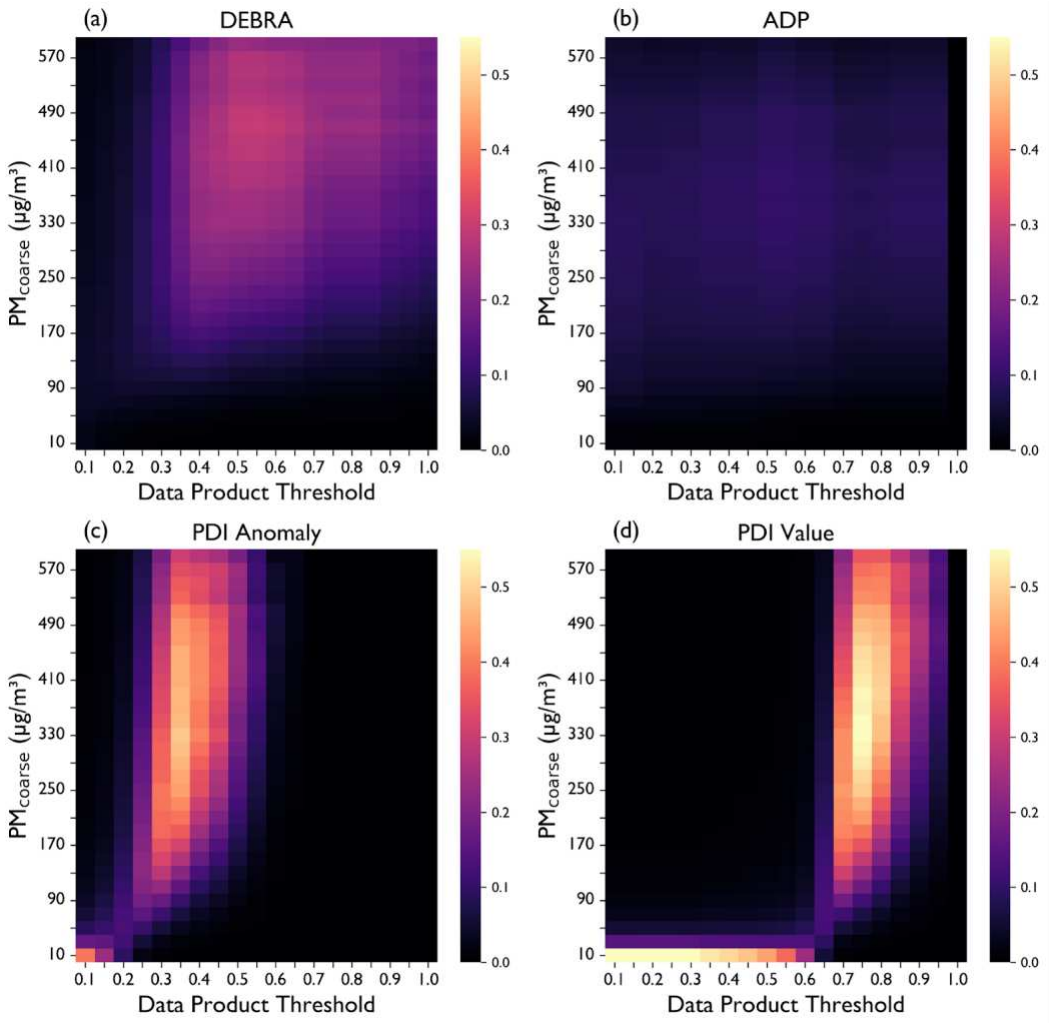

Figure A.2: F-scores with a beta of 0.25 from 2020-2023 for (a) the dynamic enhancement with background reduction algorithm (DEBRA), (b) aerosol detection product (ADP), (c) pink dust index (PDI) anomaly, and (d) PDI value.

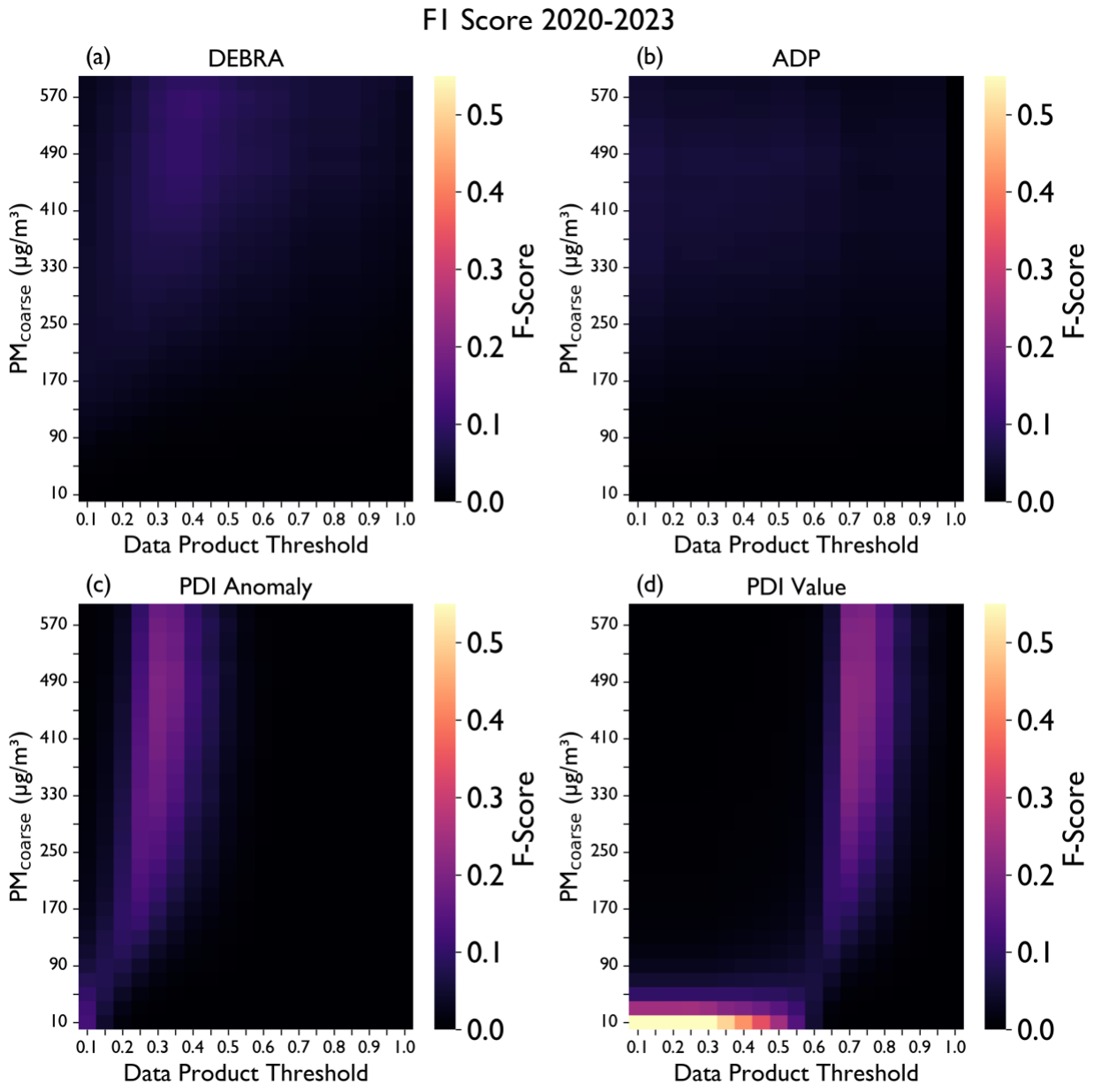

Figure A.3: F-scores with a beta of 1 from 2020-2023 for (a) the dynamic enhancement with background reduction algorithm (DEBRA), (b) aerosol detection product (ADP), (c) pink dust index (PDI) anomaly, and (d) PDI value.

Figure A.4: Desert regions with PDI values frequently >0.75 without dust plume present.

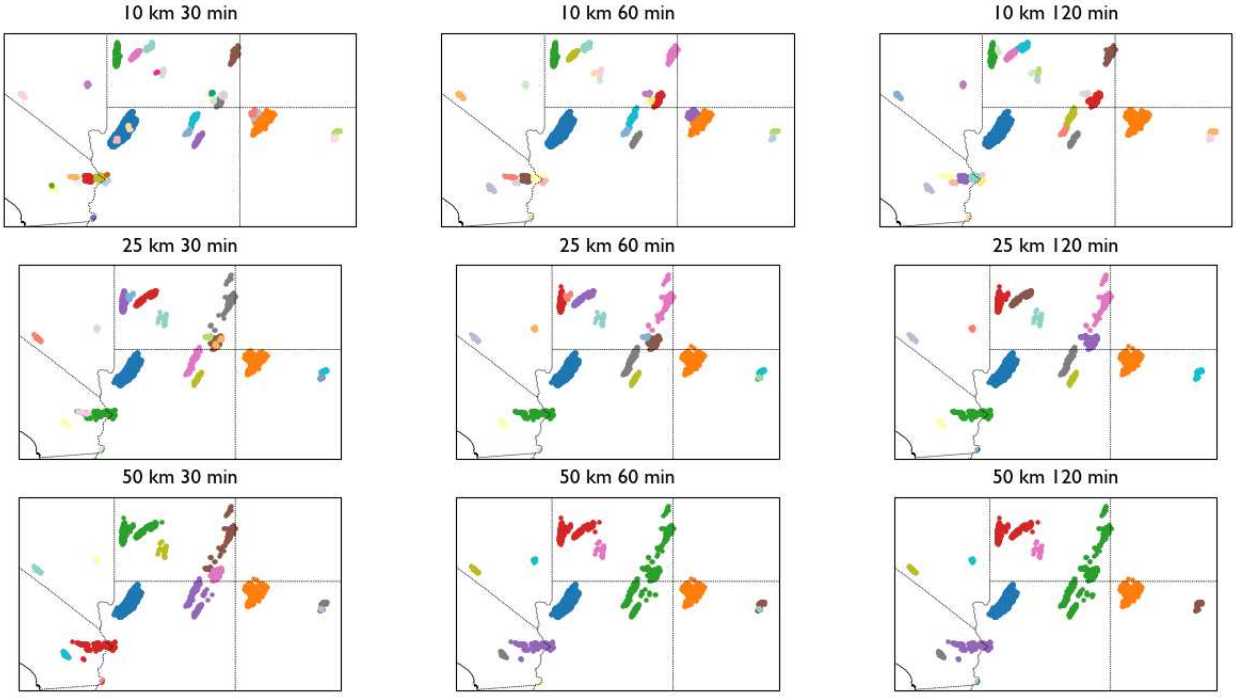

Figure A.5: Varying epsilon values through space and time on 11 May 2022 where dust plumes were present over CONUS.

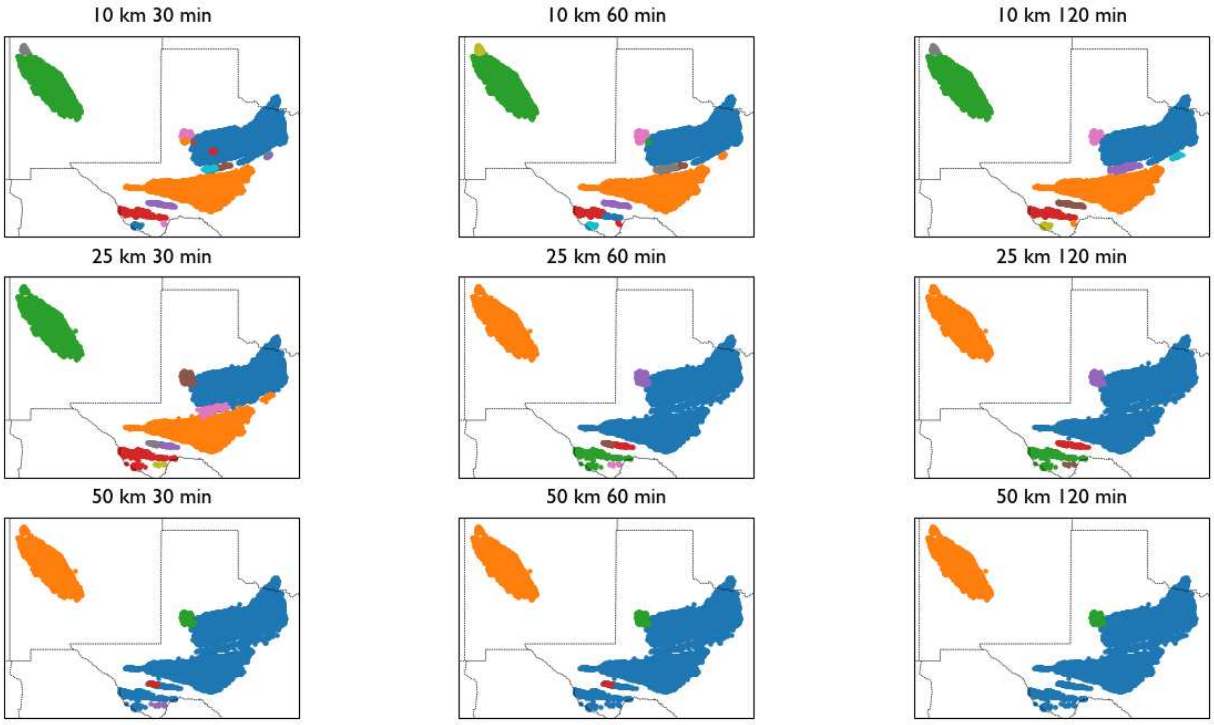

Figure A.6: Varying epsilon values through space and time on 17 March 2022 where dust plumes were present over CONUS.

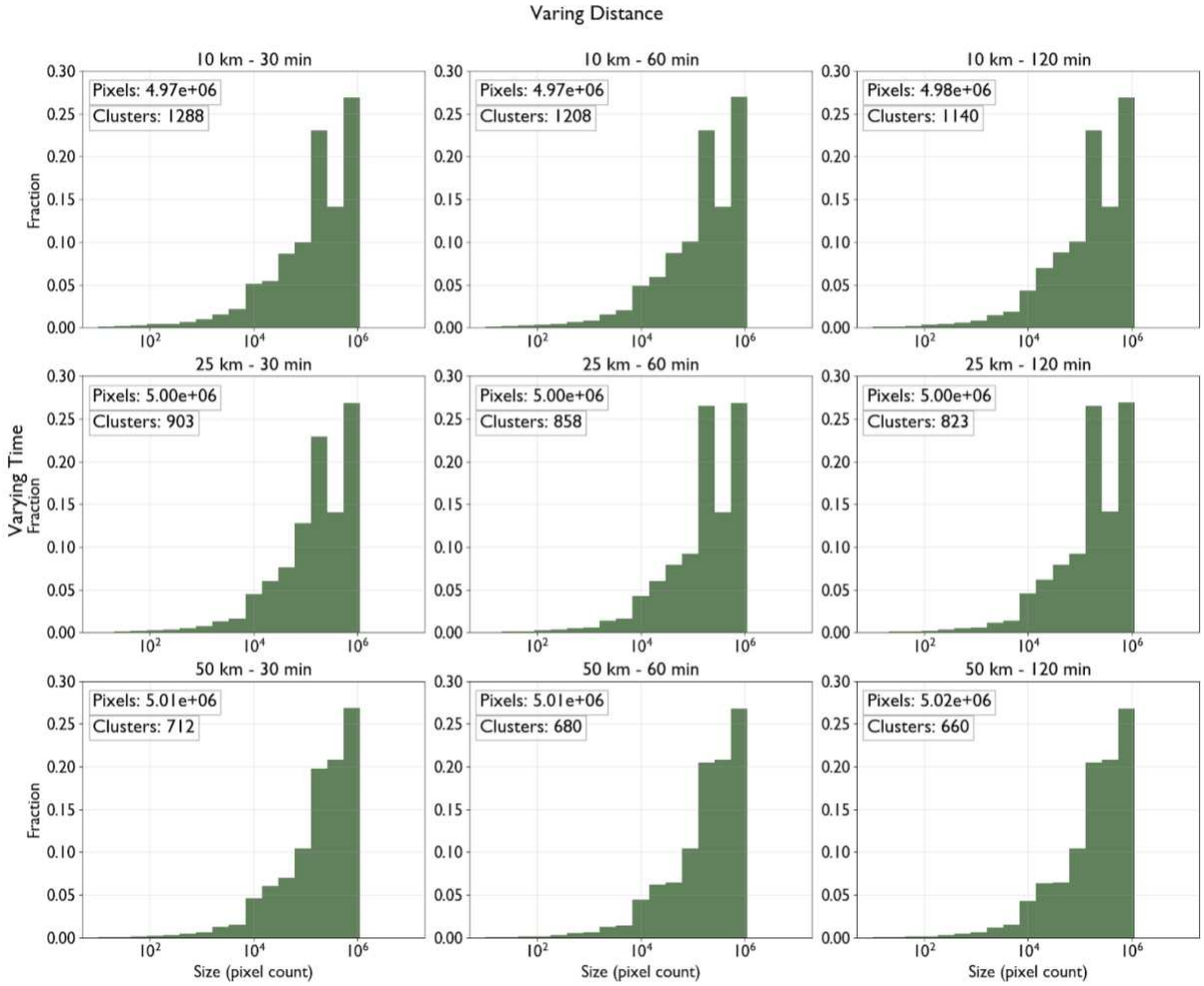

Figure A.7: Fraction of dust storm sizes varying epsilon values to investigate the total number of clusters created, the distribution of cluster sizes, and the total number of pixels included in the clusters.

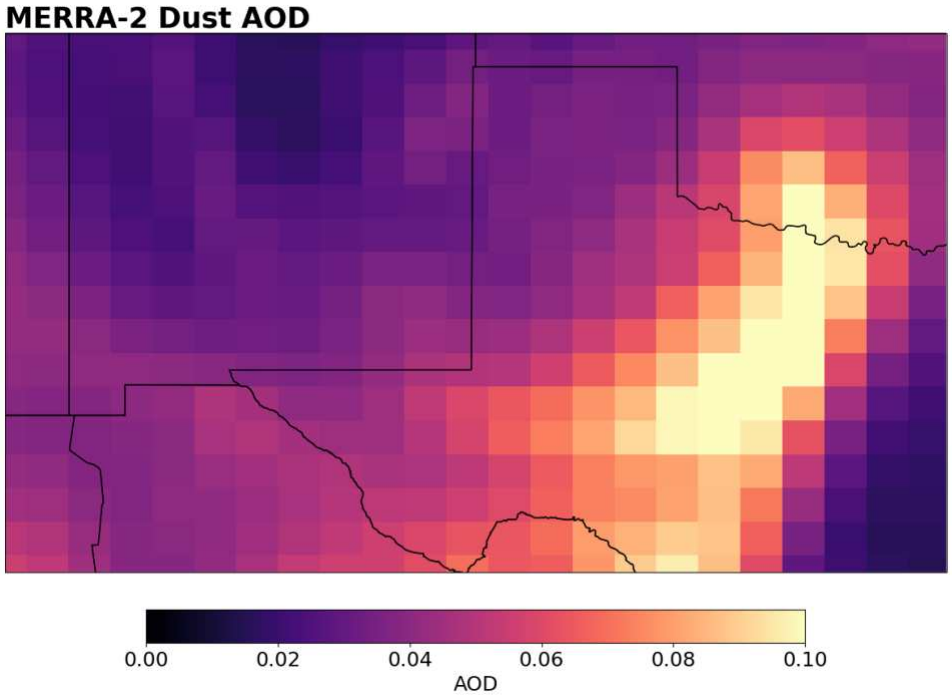

Figure A.8: Hourly Modern-Era Retrospective Analysis for Research and Applications, Version 2 (MERRA-2) dust aerosol optical depth (AOD) on 17 March 2022 22:30 UTC.

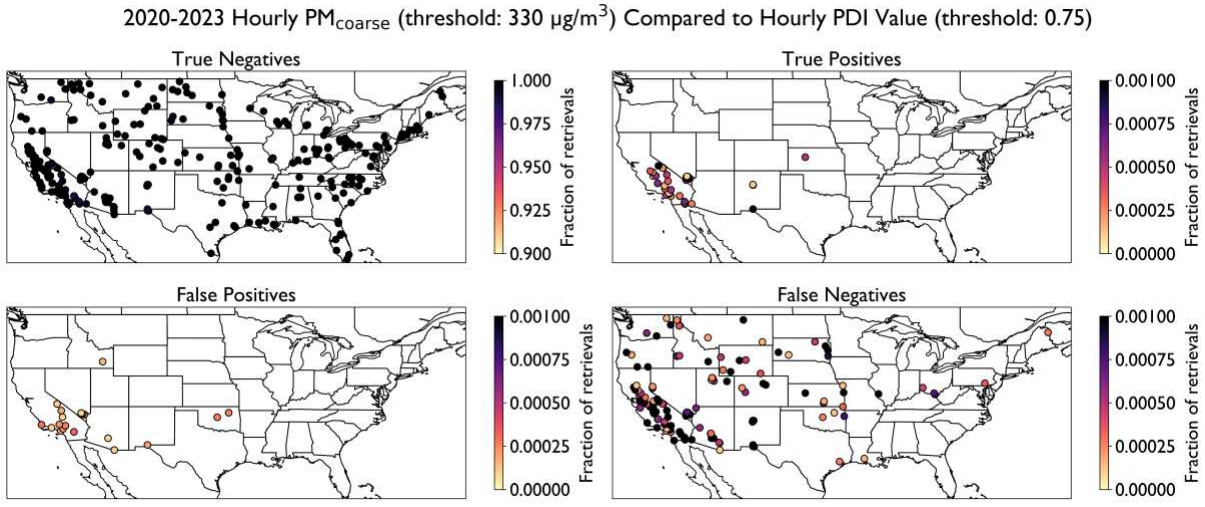

Figure A.9: Spatial distribution of PDI value true positives and negatives and false positives and negatives in the US from 2020-2023.

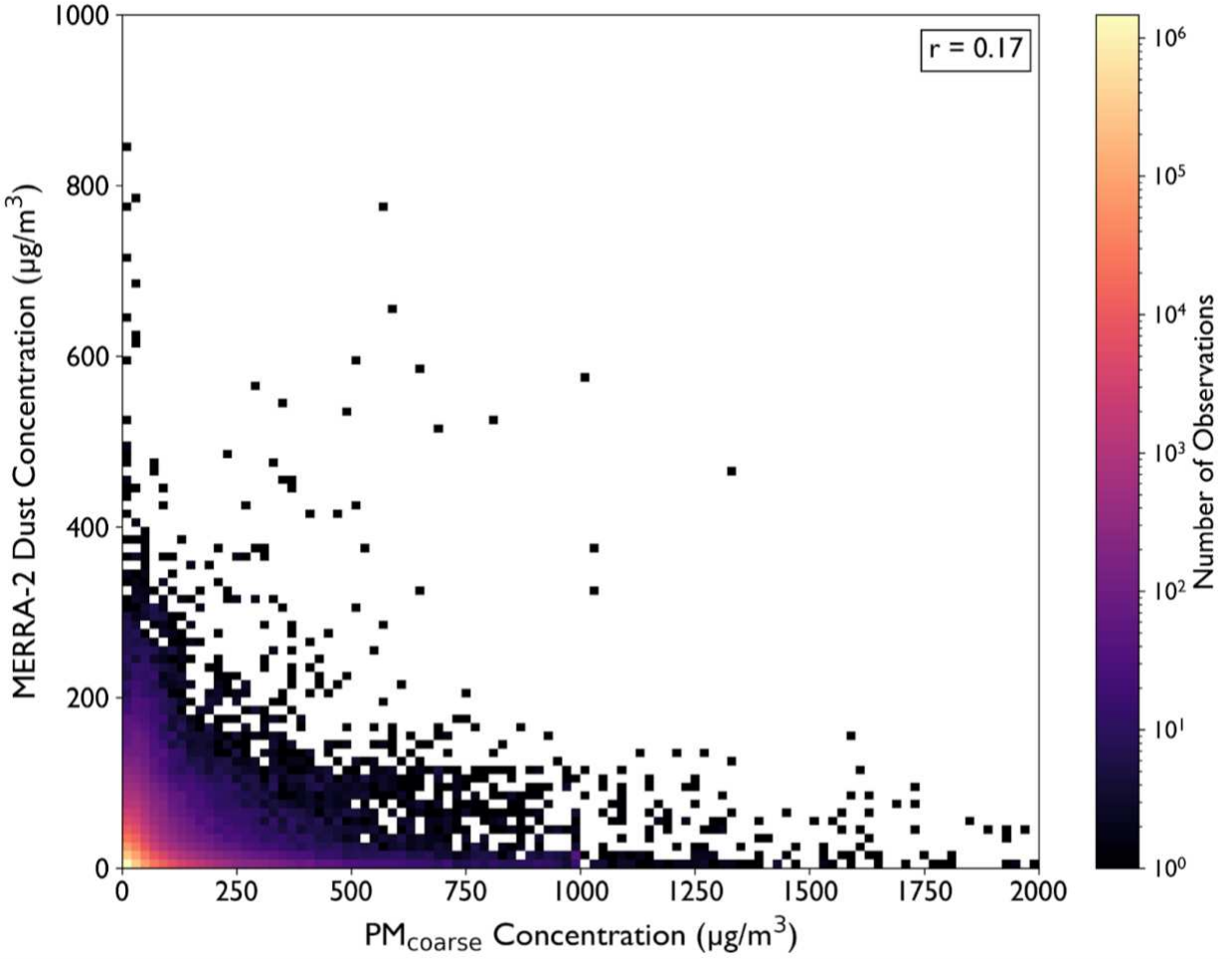

Figure A.10: 2D histogram of hourly MERRA-2 surface dust concentration vs hourly PM_{coarse} observations from 2018-2023.

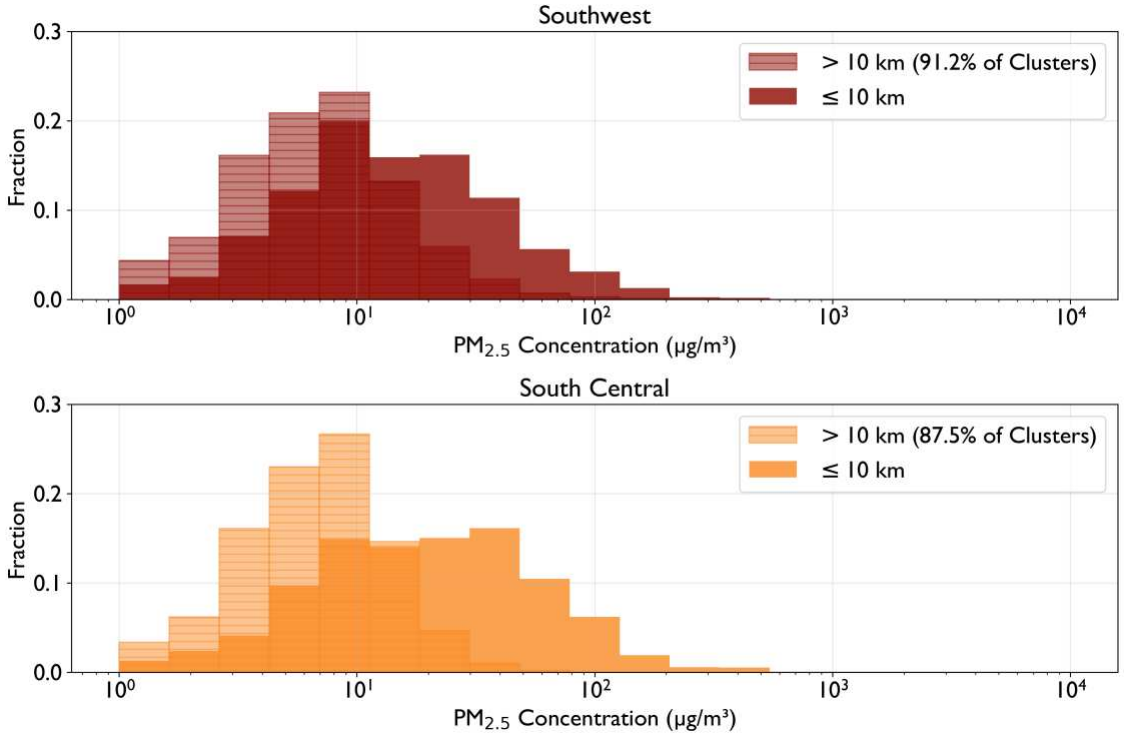

Figure A.11: Hourly $PM_{2.5}$ estimates at co-located PM_{10} and $PM_{2.5}$ monitors within 10 km of a clustered dust storm (solid bars) compared to hourly PM_{coarse} estimates at the same monitors when a cluster is not within 10 km (hatched bars).

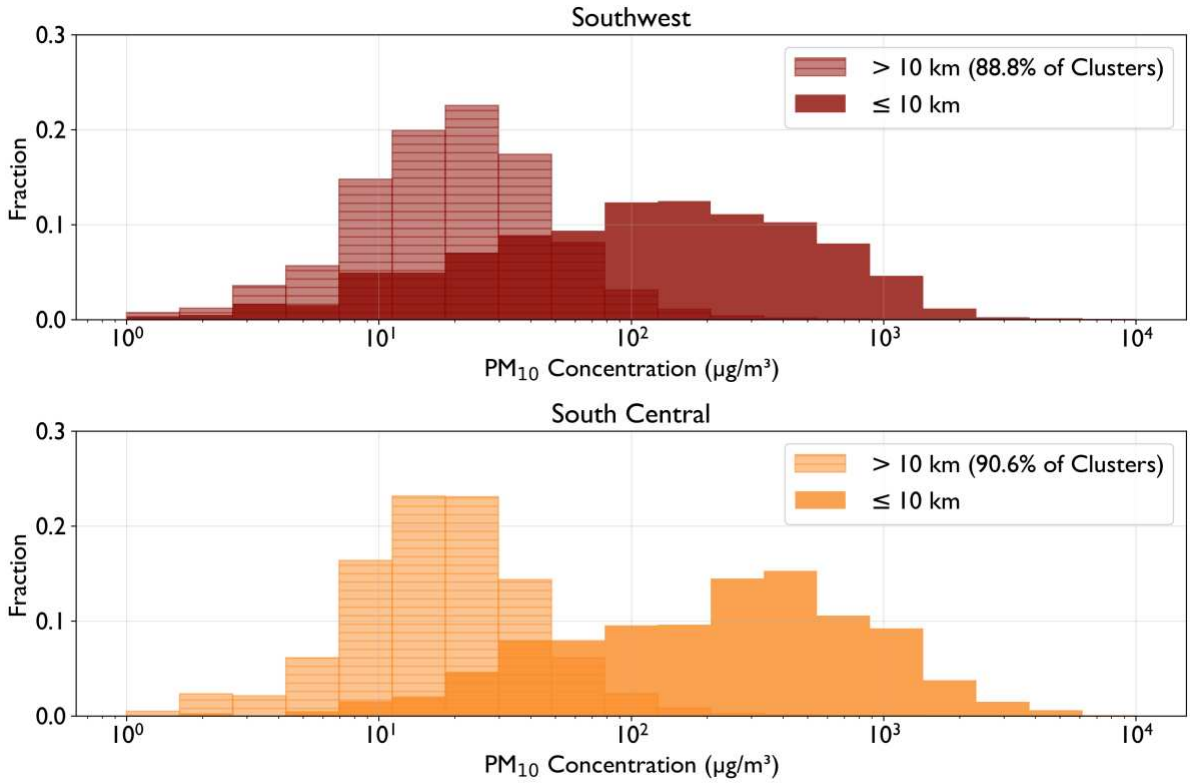

Figure A.12: Hourly PM_{10} estimates at co-located PM_{10} and $PM_{2.5}$ monitors within 10 km of a clustered dust storm (solid bars) compared to hourly PM_{coarse} estimates at the same monitors when a cluster is not within 10 km (hatched bars).